

PSFC/JA-05-33

**Spontaneous Toroidal Rotation in Alcator C-Mod Plasmas with
No Momentum Input**

Rice, J.E., Marmor, E. S., Bonoli, P. T., Granetz, R. S., Greenwald,
M. J., Hubbard, A. E., Hughes, J. W., Hutchinson, I. H., Irby, J. H.,
LaBombard, B., Lee, W., D.Lin, Y., Mossessian, D., Snipes, J. A.,
Wolfe, S. M., Wukitch, S. J.

**Plasma Science and Fusion Center
Massachusetts Institute of Technology
Cambridge MA 02139 USA**

This work was supported by the U.S. Department of Energy, Grant No. DE-FC02-99ER54512. Reproduction, translation, publication, use and disposal, in whole or in part, by or for the United States government is permitted.

Spontaneous Toroidal Rotation in Alcator C-Mod Plasmas with No Momentum Input

J. E. Rice, E. S. Marmor, P. T. Bonoli, R. S. Granetz, M. J. Greenwald,
A. E. Hubbard, J. W. Hughes, I. H. Hutchinson, J. H. Irby, B. LaBombard, W. D. Lee[†],
Y. Lin, D. Mossessian, J. A. Snipes, S. M. Wolfe and S. J. Wukitch
Plasma Science and Fusion Center, MIT, Cambridge, MA 02139-4307

[†]present address: *Archimedes Technology Group, San Diego, CA*

Abstract

Spontaneous toroidal rotation of impurity ions has been observed in the core of Alcator C-Mod plasmas with no external momentum input. The magnitude of the rotation ranges from -60 km/s (counter-current) in limiter L-mode discharges to $+140$ km/s (co-current) in ICRF heated H-mode plasmas. The core rotation in L-mode plasmas is generally counter-current and is found to depend strongly on the magnetic topology; in near double null discharges, the core rotation changes by 25 km/s with a variation of a few millimeters in the distance between the primary and secondary separatrices. In H-mode plasmas, the rotation increments in the co-current direction with the toroidal rotation velocity increase proportional to the corresponding stored energy increase, normalized to the plasma current. These discharges exhibit a positive E_r in the core. Immediately following the transition from L-mode into enhanced D_α (EDA) H-mode, the co-current rotation appears near the plasma edge and propagates to the center on a time scale similar to the energy confinement time, but much less than the neo-classical momentum diffusion time, indicating both the role of the plasma boundary in the dynamics of the H-mode transition and the anomalous nature of momentum transport. Rotation velocity profiles are flat in EDA H-mode plasmas and centrally peaked for ELM-free H-modes, demonstrating the effects of an inward momentum pinch. In EDA H-mode discharges that develop internal transport barriers (ITBs), the core toroidal rotation inside of the barrier foot is observed to drop on a time scale similar to the core pressure profile peaking (100s of ms), indicating a negative E_r well in the core

region.

I. Introduction

Rotation and velocity shear play important roles in the transition to high confinement mode (H-mode) [1-5], in the formation of internal transport barriers (ITBs) [6] and in suppression of resistive wall modes [7] in tokamak discharges. Compared to energy and particle transport, however, there has been considerably less effort addressing momentum transport. In a majority of tokamak plasmas, the toroidal rotation is generated externally by neutral beam injection. Momentum confinement is generally found to be anomalous, with a diffusivity, χ_ϕ , similar to the ion thermal conductivity, χ_i , but much larger than the neo-classical diffusivity (viscosity) [8-16].

Alcator C-Mod ion cyclotron range of frequencies (ICRF) heated [17,18] and Ohmic [17,19,20] H-mode discharges are found to have substantial spontaneous co-current toroidal impurity rotation (as high as 140 km/s, Mach number 0.3) in spite of the fact that there is no momentum input. Similar observations have been made on other devices such as JET [21,22], COMPASS [23] and Tore Supra [24-26]. In L-mode, the rotation has been found to be in the counter-current direction [27], with the magnitude depending strongly on magnetic configuration [28,29], which may be related to the higher H-mode power threshold observed when the X-point is positioned away from the ion $\mathbf{B} \times \nabla B$ drift direction.

In future devices which may not have neutral beam injection to generate plasma rotation (and the many beneficial effects of rotation), control of spontaneous rotation may provide the solution. In order to gain a better understanding of the mechanism generating the rotation in the absence of an external source, and in general to characterize momentum transport, temporally resolved velocity profiles are needed. In the absence of neutral beam based diagnostics, a new tangentially viewing x-ray spectrometer array [28] has been installed on Alcator C-Mod in order to provide this information. An outline of this paper is as follows: a brief description of the experiment and the spectrometer array is provided in II. Observed rotation for L-mode discharges in a variety of magnetic configurations is given in III. Rotation profile evolution in H-mode plasmas is presented in IV, in addition to scalings with

plasma parameters and the connection to the H-mode transition. Comparisons with neo-classical theory are made in both Sections. Rotation observations in ITB plasmas are shown in V and comparisons with various rotation theories are given in VI. A discussion and conclusions are presented in VII.

II. Experiment and Spectrometer Description

Alcator C-Mod [30] plasmas have been formed in a variety of magnetic topologies: lower single null (LSN), double null (DN), upper single null (USN) and inner wall limited. Auxiliary heating is available with 4 MW of ICRF heating power at 80 MHz, which is coupled to the plasma by 2 two-strap antennas. For the plasmas described here, the hydrogen minority heating was with $0 - \pi$ phasing, and theoretically, there was no momentum input. An additional 4 MW of ICRF power are available with variable frequency between 50 and 80 MHz from a variable phase four-strap antenna; for the cases described here, this antenna was operated with $0 - \pi - 0 - \pi$ phasing, again with no momentum input. Core toroidal rotation measurements are provided from the Doppler shifts of argon and molybdenum x-ray lines recorded by an array of von Hamos type x-ray crystal spectrometers [31]. The current system has three vertically scanable spectrometers with a near radial view and three fully tangential viewing spectrometers, vertically displaced to provide three points on the rotation profile. The spectrometer arrangement around the device is shown in Fig.1. The three spectrometers at C, F and K ports have views which are tangent to $R=0.685$ m; the C port spectrometer is on the mid-plane while the F and K port spectrometers are vertically displaced by 0.09 and 0.18 m, respectively, providing profile coverage of toroidal rotation at $r/a = 0.0, 0.3$ and 0.6 . The central chord spectrometer observes the Ar^{17+} Ly_α doublet while the off-axis spectrometers monitor the Ar^{16+} forbidden line, z [17]. Time resolution for the central spectrometer is 20 ms, while for the other two is 50 ms. Statistical errors in the deduced rotation velocities from fits to the line positions depend on the counting rate and are usually less than 5×10^3 m/s. These three rotation measurements

are augmented by the velocity of magnetic perturbations associated with sawtooth oscillations recorded with an array of fast pickup coils [19]. This provides rotation information at the $q=1$ surface, which is typically near $r/a \sim 0.2$. For all of the discharges presented here, the observed sawtooth inversion radii were in the range of $0.17 \leq r/a \leq 0.23$. Rotation velocities of main ions in the scrape-off layer (SOL) are available from a variety of Mach probes [29]. Core poloidal rotation information is provided by the vertically scanning, nearly radially viewing x-ray spectrometers recording argon impurity Doppler shifts at B port. Electron density profiles were determined by Thomson scattering and from the visible continuum using a high spatial resolution imaging CCD system [32]. Electron temperature profiles were determined from Thomson scattering and from electron cyclotron emission (ECE). Central ion temperatures were obtained from neutron flux measurements while ion temperature profile information is available from Doppler broadening of argon x-ray lines. Magnetic flux surface reconstructions were provided from the EFIT [33] code.

III. Observed Rotation in L-mode Plasmas

Shown in Fig.2 are x-ray spectra [27] from the core ($r/a = 0.0$) of two similar Ohmic L-mode discharges, including the argon [34] and molybdenum [35] lines used for the rotation analysis. The thin vertical line indicates the rest wavelength for $\text{Ar}^{17+} \text{Ly}_{\alpha 1}$. The spectrum on the left (dash-dot line) is from a plasma with the current in the counter-clockwise direction. Since the spectrometer views counter-clockwise (see Fig.1, C-port), and the spectrum is blue-shifted, the impurities (argon and molybdenum) were rotating clockwise, in the same direction as the electrons, opposite to the plasma current (counter-current). The magnitude of the shift was $\sim 0.5 \text{ m}\text{\AA}$, which yields a toroidal rotation velocity of $(0.5 \text{ m}\text{\AA}/3731.1 \text{ m}\text{\AA}) \times c = 4 \times 10^4 \text{ m/s}$, in the counter-current direction. The spectrum on the right (shown by the solid curve) is from a reversed (clockwise) current plasma, the spectrum is red-shifted by about the same amount, and the impurities were rotating counter-clockwise, again in the same direction as the electrons, counter-current.

The rotation of argon and molybdenum ions is very similar, which is demonstrated in Fig.3, where the rotation velocities deduced from Ar¹⁷⁺ and Mo³²⁺ are shown as a function of time for a lower single null (LSN), Ohmic L-mode discharge. The line brightness time histories for these two lines were very different. The molybdenum signal was strongest in the early portion of the discharge [36] around 100 ms, when the plasma was in contact with the molybdenum walls and before the plasma was diverted, and then dropped substantially during the high density portion of the discharge when the electron temperature was lowest. In contrast, argon is usually injected at 300 ms into the discharge, so the signal before that time is very low, and then increases and holds steady at an ample level for line fit analysis for the remainder of the discharge. The rotation velocity time histories for these two ions, however, were nearly the same.

A comparison of rotation time histories for LSN, Ohmic L-mode discharges with normal and reversed plasma current is shown in Fig.4. (Hereafter all impurity rotation velocities shown will be from argon ions unless otherwise noted.) In both cases, the magnitude of the rotation was largest at the beginning of the discharge when the loop voltage was highest and the density was low, and then decreased as the discharge developed. These velocity time histories have been compared with the predictions of neo-classical theory. Neo-classical toroidal rotation has been calculated [37] from the electron, ion and impurity parallel momentum and heat flow balance equations [38], under the assumption of no net momentum input, appropriate for Ohmic discharges. The expression for the central toroidal impurity rotation velocity, assuming that the total momentum is zero, is given as (from Eq.56, Ref.[37])

$$V_{Tor}^I = 4.19 \times 10^3 f \frac{Z_i}{\sqrt{\mu}} \frac{V_l}{R} \frac{T_i^{3/2}}{n_i} \quad (m/s). \quad (1)$$

Z_i is the charge of the background ion, μ is the mass of the background ion in amu, V_l is the loop voltage in volts, R is the major radius in m, T_i is the ion temperature in keV, n_i is the ion density in $10^{20}m^{-3}$ and

$$f = \frac{Z_I - Z_i}{Z_I} \frac{\sqrt{2} + 13\alpha/4}{(1 + \alpha)(\sqrt{2} + \alpha)} \frac{n_i m_i}{n_i m_i + n_I m_I}. \quad (2)$$

Z_I is the charge of the impurity ion, n_I is the impurity ion density, m_I is the impurity ion mass, m_i is the background ion mass, and $\alpha \equiv n_I Z_I^2 / n_i Z_i^2$. f is of order 1 for typical Alcator C-Mod conditions, with deuterium as the majority ion, and nominal maximum values for the impurity concentration n_I/n_i are 2×10^{-4} ($\alpha=0.2$) for molybdenum [36] and 3×10^{-4} ($\alpha=0.09$) for argon. A comparison of the calculated rotation from Eqns.1 and 2 is made with the measured time histories by the dashed curves in Fig.4. The calculations are in reasonable agreement with the observations, correctly predicting the direction of the rotation and the independence on impurity mass.

In discharges with locked modes, the toroidal rotation has been observed to stop [39,40]. Similar behavior has also been seen in C-Mod plasmas [28]. Shown in Fig.5 are parameter time histories for an Ohmic L-mode discharge which developed a locked mode at ~ 0.96 s. The locked mode formation was accompanied by a drop in stored energy and electron temperature, disappearance of sawtooth oscillations and a braking of the toroidal rotation velocity. These modes occur in C-Mod plasmas with low density and high plasma current. In this particular case, all of these symptoms developed at about the same time.

The ambient core L-mode toroidal rotation velocity during the steady state phase of LSN discharges has been found to be in the range between -5 and -25 km/s [27,17,18,28]. Here, the minus sign indicates counter-current rotation. The core L-mode rotation velocity as a function of electron density for 5.4 T, 0.8 MA discharges is shown in Fig.6. For LSN plasmas (dots) with the ion $\mathbf{B} \times \nabla B$ drift downwards, there is little variation with electron density. For upper single null (USN) discharges (asterisks), the core rotation is considerably more counter-current [28,29] for electron densities above $1 \times 10^{20}/\text{m}^3$, while the rotation is the same in both configurations below this value. Related differences in rotation velocities have been found in the SOL [29]. SOL flows provide the boundary conditions for rotation

in the core, which propagates in on the momentum diffusion time scale, and which is comparable to the energy confinement time (see next section). Interestingly, the density for which the rotation is the same in the two configurations is very close to the H-mode density threshold for 5.4 T and 0.8 MA: below this density, H-modes are not accessible with the available ICRF power of 5 MW. There are also points from inner wall limited discharges which exhibit strong counter-current rotation, similar to the USN discharges.

The magnetic configuration has been changed dynamically during the course of plasma discharges and the rotation has been seen to become more counter-current when the X-point is moved to the top. This is demonstrated in Fig.7, which shows a comparison of two otherwise similar discharges which began with a LSN then switched to USN. In the bottom frame is the distance between the primary and secondary separatrixes (SSEP), mapped to the midplane. When SSEP is negative, the plasma has a LSN, when SSEP is 0, the discharge has a double null and when SSEP is positive, there is an USN. The only difference between these two discharges was the timing of the USN transition. When each plasma switched to USN, there was a significant drop (an increase in the counter-current direction) in the central rotation velocity. These discharges both had the ion $\mathbf{B} \times \nabla B$ drift downward.

The core rotation velocity has been found to be extremely sensitive to SSEP, as suggested in Fig.7, and is shown in Fig.8 for a series of near double null (DN) 5.4 T, 0.8 MA discharges with an electron density of $1.4 \times 10^{20}/\text{m}^3$. The core rotation velocity falls by 25 km/s with an SSEP variation of a few mm. Similar sensitivity has been observed in the SOL [29].

IV. Observed Rotation in H-mode Plasmas

Rotation in (ICRF and Ohmic) H-mode plasmas has been found to be in the co-current direction [17-20,41,28]. The time histories of plasma parameters for a LSN discharge with the ICRF power level well above the H-mode threshold are shown in Fig.9. Prior to the ICRF pulse, this 1.0 MA, 5.7 T hydrogen minority deuterium

(D(H)) discharge had a central electron density of $2.3 \times 10^{20}/\text{m}^3$ and was rotating at about 1×10^4 m/s in the counter-current direction. Well into the ELM-free H-mode after 1 second with 3.2 MW of ICRF power, the electron density rose to $4.4 \times 10^{20}/\text{m}^3$ and the central argon toroidal rotation velocity increased to 1×10^5 m/s in the co-current direction. While the time histories of the stored energy and the toroidal rotation are very similar, there is a slight delay in the rotation (for example in the dip around 0.85 s), which indicates that the central rotation is an effect of the improved confinement rather than the cause. The rise time of the central rotation (and decay time) is typically 50-100 ms [17], similar to the energy confinement time in H-mode [42]. Throughout this discharge, the impurity strength parameter α , defined as $n_I Z_I^2/n_i Z_i^2$, was less than 0.007. Impurity rotation velocity profiles [17] for a series of ELM-free ICRF H-mode plasmas, similar to that shown in Fig.9 are shown in Fig.10. These profiles have been compared to the computed neo-classical profiles. Theoretical expressions for the neo-classical impurity and majority ion toroidal and poloidal rotation velocities are given by Eqns.(37), (38), (33) and (34), respectively, of Ref.[37]. These expressions were obtained by solving the parallel momentum and heat flow balance equations, including one impurity species. No effects of ion orbit shifts have been included, nor have been the individual charge states for the impurity species. These rotation velocities may be written (in the absence of a parallel electric field) as

$$V_T^I = \frac{1}{B_P} \left[E_r + \frac{(K_1 + \frac{3}{2}K_2 - 1)}{e} \frac{\partial T_i}{\partial r} - \frac{T_i}{en_i} \frac{\partial n_i}{\partial r} \right] \quad (3),$$

$$V_T^i = \frac{1}{B_P} \left[E_r + \frac{(K_1 - 1)}{e} \frac{\partial T_i}{\partial r} - \frac{T_i}{en_i} \frac{\partial n_i}{\partial r} \right] \quad (4),$$

$$V_P^I = \frac{1}{B_T} \left[\frac{(K_1 + \frac{3}{2}K_2 - 1)}{e} \frac{\partial T_i}{\partial r} - \frac{T_i}{en_i} \frac{\partial n_i}{\partial r} + \frac{T_I}{Z_I en_I} \frac{\partial n_I}{\partial r} \right] \quad (5)$$

and

$$V_P^i = \frac{1}{B_T} \frac{K_1}{e} \frac{\partial T_i}{\partial r} \quad (6).$$

Here the subscripts T and P denote toroidal and poloidal, e is the electric charge, B is the magnetic field, T and n are the temperature and density, K_1 and K_2 are functions of the viscosity matrix elements, inverse aspect ratio and the impurity strength parameter (evaluated for all collisionality regimes in the appendix of Ref.[37]) and E_r is the radial electric field. Note that the V_P s are independent of E_r . Eqn.(3) (and Eqns.(4-6)) is very weakly dependent on the impurity species in Alcator C-Mod plasmas; for low values of α , the expressions for K_1 and K_2 are insensitive to the impurity mass. The rotation velocities in Eqns.3 and 5 have been evaluated from the observed electron temperature profiles (the ion temperature profiles are taken to be the same for this high density plasma), the measured electron density profiles (the ion density profiles are taken to be the same for this low Z_{eff} plasma), the measured argon density and temperature (from the intensities and widths of the Ar^{16+} lines [43]) and the magnetic field and q profiles calculated from the magnetics diagnostics using EFIT. The only quantity not directly measured in Eqns.(3) is E_r . The calculated argon toroidal and poloidal rotation velocity profiles from Eqns.(3) and (5) (E_r is again not included in the toroidal velocities) are shown in Fig.10. The argon (impurity) and deuteron (ion) poloidal rotation velocities near the edge are not expected to be the same, and this has been observed in DIII-D [44]. The measured core value for the argon poloidal rotation velocity is $0 \pm 3 \times 10^3$ m/s, consistent with the calculations. (This justifies ignoring $V_P B_T / B_P$ compared to V_T .) The measured toroidal rotation velocity profile has been used with Eqn.(3) to determine E_r , with typical values of order +30 kV/m [17] in the core.

The rotation velocity during ICRF heating does not seem to be a strong function of the impurity mass. The occurrence of a Mo^{32+} line at 3739.8 mÅ [35] in the same spectrum with the Ar^{17+} doublet allows a comparison of the rotation velocities of impurities with substantially different masses to be made, as in Fig.3 for L-mode plasmas. Shown in Fig.11 are the rotation velocity times histories for

molybdenum (100 AMU) and argon (40 AMU) from a 0.85 MA, 5.7 T, H-mode discharge. The rotation velocities of these two ions are very similar during the 2.7 MW ICRF pulse, indicating that impurity diamagnetic effects are unimportant for low impurity densities. (Note the delay between the rises and falls of the rotation signals relative to the ICRF waveform.) The charge to mass ratios for these two ions are .32 for Mo and .42 for Ar. Argon and molybdenum rotation velocities are also the same during Ohmic L-mode discharges (see Fig.3).

Shown in Fig.12 is a comparison of the central impurity toroidal rotation velocity in two similar H-mode discharges that had normal and reversed plasma current (top frame). Both plasmas had on-axis heating with comparable ICRF power levels (third panel) and subsequent stored energy increases (second frame); the changes in the rotation velocities (bottom panel) were of similar magnitude but in opposite directions, remaining co-current. The time histories of the rotation velocities were very similar to the plasma stored energy time histories, although for the reversed current case the rotation velocity was ‘negative’. (Compare with Fig.4 in L-mode.) There was a delay, about equal to the energy confinement time, of the modulations in the velocity traces relative to the stored energy signals. In otherwise similar plasmas with comparable stored energy increases after the transition to H-mode, the toroidal rotation is higher in plasmas with lower plasma current. This effect is demonstrated in Fig.13, where the time histories of the plasma current, stored energy and rotation velocity are shown for two D(H) discharges at 5.4 T with 2.5 MW of ICRF power between 0.6 and 1.2 s. The stored energy increase during the ICRF pulse in both cases was about 45 kJ, although the 1 MA plasma had a higher stored energy target plasma before 0.6 s. The 600 kA plasma rotated about a factor of two faster compared to the higher current case. Another perspective on this effect is illustrated in Fig.14. In the top of the figure are the discharge trajectories in the Stored Energy - Rotation Velocity plane of three similar discharges each at 0.6 and 1.0 MA. Both sets of plasmas began at the same velocity, and reached the same velocity throughout the ICRF pulse, around 4×10^4 m/s, whereas the peak stored energy in the higher current plasmas was almost twice as large. In the bottom

of the figure are the same trajectories, with the stored energy normalized to the plasma current, which brings the two sets of discharges on top of each other. Scaling of the rotation velocity with β_P instead of W_P/I_P is not as good since an I_P^{-2} dependence is too strong. The relationship between the rotation velocity, stored energy and plasma current is summarized in Fig.15; this is a comparison between the rotation velocity increase before and during ICRF and Ohmic H-modes and the plasma stored energy increase normalized to the plasma current, before and during ICRF and Ohmic H-modes [41]. All of the ICRF data are for plasmas with the resonance close to the magnetic axis. The ICRF H-mode points are sorted by plasma current; there is a larger velocity increase for a given stored energy increase at lower plasma current. The Ohmic H-mode points display a similar trend, although the stored energy increases are modest since with only Ohmic power input, it is difficult to exceed the H-mode threshold. The Ohmic points have not been sorted by plasma current, but the range presented in the figure is from 0.8 to 1.4 MA, which also explains why the rotation velocity increases are modest compared to the ICRF points. This common trend suggests that the co-current toroidal rotation is probably not driven by the ICRF waves or energetic particle effects. Similar rotation velocities and scaling with stored energy have been observed in sawtooth pre- and post-cursors from the magnetics diagnostics [19,20].

Rotation velocity profile evolution following the H-mode transition has been determined from the array of tangentially viewing spectrometers (Fig.1). Shown in Fig.16 (top) are the time histories of the (impurity) toroidal rotation velocities at three radii for a 2.0 MW ICRF heated EDA H-mode [42] plasma. This 0.8 MA, 5.3 T discharge entered EDA H-mode at 1.11s. The velocity increase was first seen on the outermost spectrometer ($r/a = 0.6$), sequentially moving inward, suggesting an edge source of toroidal momentum which propagated in towards the center, with a time scale somewhat longer than τ_E , the energy confinement time. After about 200 ms (at 1.3 s), the rotation settled to a value of ~ 50 km/s (in the co-current direction), with a flat profile. During this steady phase of the discharge, the central electron density was $2.8 \times 10^{20}/\text{m}^3$ and the central electron temperature was 2.1

keV. Similar velocity profile evolution has been seen in purely Ohmic EDA H-mode plasmas. This time evolution and flat steady state rotation profile suggest that the momentum transport in EDA H-mode plasmas may be characterized by a purely diffusive process. The situation is different in ELM-free H-mode plasmas, as can be seen in the bottom of Fig.16. This 0.8 MA, 4.6 T discharge entered ELM-free H-mode at 0.624 s, reverted to L-mode at 0.834 s, then re-entered ELM-free H-mode at 0.871 s. Following both L-H transitions, there was a rapid increase in the core rotation velocity and stored energy. In contrast to the EDA H-mode case, these rotation profiles are highly peaked, reaching ~ 70 km/s in the core (again in the absence of external momentum input) and ~ 15 km/s at $r/a=0.6$. For such a profile to be sustained in steady state in the presence of momentum diffusion without a central momentum source requires there to be a mechanism of inward momentum transport up the velocity gradient, an inward momentum pinch [13]. During the first ELM-free period, the electron temperature was relatively constant at 1750 eV, while the electron density rose continuously from 1.1 to $2.9 \times 10^{20}/\text{m}^3$, but maintaining a flat profile. Improved energy, particle and impurity confinement is a characteristic of ELM-free discharges; whether this momentum peaking is related is an open question. Excessive radiation from unabated electron density increase and impurity accumulation limits the duration of ELM-free H-mode plasmas. In contrast, EDA H-mode discharges have nearly as good energy confinement, but the relatively higher particle diffusivity allows for steady state electron density profiles and no radiation problems. These H-mode confinement regimes are discussed in detail in the previous Chapter II.

The evolution of the toroidal rotation velocity profiles has been simulated using a simple source-free momentum transport model [16]

$$\frac{\partial}{\partial t}P + \text{grad}(-D_\phi \frac{\partial}{\partial r}P - v_\phi P) = 0 \quad (7)$$

with $P = n_i m_i V_\phi$ and $v_\phi = v_c r/a$, where a is the minor radius and where the momentum diffusivity, D_ϕ , and the momentum convection velocity, v_c , are free parameters to be determined. Positive v_c indicates inward convection. Subject to the boundary

conditions of an edge rotation, V_0 , which is present only during H-mode ($V_\phi(a,t) = V_0$ during H-mode, and 0 otherwise) and with the assumptions (observed in the electrons) of a flat ion density profile and constant (spatially and temporally) D_ϕ and v_c , the toroidal rotation velocity, V_ϕ , profile evolution may be determined (in cylindrical coordinates) from a solution to

$$\frac{\partial}{\partial t} V_\phi - D_\phi \left[\frac{\partial^2}{\partial r^2} V_\phi + \left(\frac{1}{r} + \frac{v_c r}{a D_\phi} \right) \frac{\partial}{\partial r} V_\phi + \frac{2v_c}{a D_\phi} V_\phi \right] = 0 \quad (8)$$

via an expansion in confluent hypergeometric functions.

An example of a comparison of this model to the observed velocity time evolution in the EDA plasma is shown by the curves in the top frame of Fig.16; the three curves represent the simulated rotation velocities at the radii of the three spectrometer views. For this case, D_ϕ was spatially constant with a value of 0.05 m²/s, and $v_c \approx 0$, which corresponds to a momentum confinement time, τ_ϕ , of 150 ms. This momentum diffusivity is much greater than the neo-classical viscosity [45], $\chi_\phi \sim \rho_i^2 / \tau_{ii} \sim 0.003$ m²/s for this case, and the momentum transport may be characterized as anomalous. The momentum diffusivity may also be determined for L-mode from the decay of the rotation velocity after the H- to L-mode transition at 1.53 s; D_ϕ for the L-mode portion of this discharge was 0.20 m²/s, with $\tau_\phi \sim 35$ ms. From modeling of several ICRF and Ohmic EDA H-mode plasmas, D_ϕ was found to be in the range from 0.05 to 0.10 m²/s, with $v_c \approx 0$, and τ_ϕ in the range from 70-150 ms. The simulations for the ELM-free discharge are shown in the bottom frame of Fig.16, which is on the same time scale as the top frame for comparison. In this instance D_ϕ was 0.40 m²/s with $v_c = 12$ m/s, and $\tau_\phi \sim 70$ ms. This value of the pinch velocity was necessary to match the quasi-steady peaked profile shape at 0.8 s, with a ‘peaking factor [46]’, $S \equiv a v_c / 2 D_\phi = 3.2$, along with the overall rise time of the rotation. From the rotation decay after the H- to L-mode transition (from 0.82-0.88 s), a value of $D_\phi \sim 0.25$ m²/s was determined. From the rotation decays in many discharges after the H- to L-mode transition (both EDA and ELM-free), D_ϕ for L-mode was determined to be in the range from 0.20-0.25 m²/s, with $v_c = 0$.

Shown in Fig.17 are the time histories of several parameters of interest for an

Ohmic H-mode plasma. This H-mode was achieved by operating at relatively high plasma current (1.1 MA), in order to increase the total input power, and by ramping down the toroidal magnetic field from 5.4 to 4.3 T, in order to lower the H-mode threshold, which has been determined to scale as B_T . This plasma entered H-mode at 0.82 s, when the D_α signal dropped, and the plasma stored energy, the electron density (and temperature) and the central rotation velocity all increased. During the H-mode period, the plasma stored energy nearly doubled, reaching 105 kJ, the central electron density also doubled, increasing to $4.2 \times 10^{20}/\text{m}^3$, while the central toroidal rotation velocity exceeded 3×10^4 m/s. Nearly identical rotation has been observed in sawtooth pre- and post-cursors measured with magnetic pick-up coils [19,20]. The similar evolution of the rotation in Ohmic and ICRF H-modes suggests that the mechanism generating the rotation in the absence of external momentum input has nothing to do with ICRF wave or energetic particle effects.

The role of rotation in the dynamics of the H-mode transition has been investigated in different magnetic topologies, all with the ion $\mathbf{B} \times \nabla B$ drift downwards. A comparison of H-mode discharges in three different magnetic configurations (LSN, DN and USN) with the minimum ICRF power necessary to induce the transition is shown in Fig.18. The times have been shifted so that the H-mode transition time is at 0 s. In the USN case, there is an evolution (increase) of the edge electron temperature and gradient (actually $\nabla P_e/n_e$), and core rotation velocity before the H-mode transition on a time scale (~ 150 ms) longer than the energy confinement time. (ITBs in C-mod evolve on a similar time scale [41,47-49].) During this time the electron density and gradient remained constant. In all three configurations the transition occurred about when the core rotation velocity crossed through 0 km/s. This does not imply that the core rotation velocity passing through 0 km/s is a condition for the transition; it is most likely the edge velocity or gradient (or E_r gradient) which must reach a certain value. The edge rotation velocity and gradient are not routinely measured on C-Mod, whereas the core rotation is readily available, and with good time resolution. Since the core rotation has been shown to be strongly coupled to the edge value, with the rotation propagating in to the

center following the EDA H-mode transition with a momentum diffusion time scale similar to the energy confinement time [16,28], the core rotation is a good indicator of the edge rotation. For the particular set of conditions for the target plasmas in Fig.18, 0.8 MA, 5.4 T and average electron density of $1.4 \times 10^{20}/\text{m}^3$, the H-mode transition occurred when the core velocity passed through 0. The edge electron temperature (and gradient) was a factor of two higher at the H-mode transition in the USN case, compared to LSN, as has been previously reported [50]. With a stronger counter-current rotation in USN, more ICRF power was required to raise the stored energy (see Fig.15), and hence the rotation velocity from -50 km/s to 0 km/s, thus the higher H-mode power threshold.

The H-mode power threshold has been carefully determined as a function of SSEP. Shown in Fig.19 are the ambient L-mode core rotation velocities as a function of SSEP (similar to Fig.8) for the standard discharge conditions, and the minimum additional ICRF power required for these discharges to achieve H-mode. The shapes of the trends are opposite, with the rotation velocity and threshold power being very sensitive to SSEP in near DN plasmas. There are more points in the top panel because not all of these discharges had enough ICRF power to enter H-mode. Models of the H-mode power threshold and its dependence on magnetic topology should take into account the variations of plasma rotation with magnetic topology in L-mode.

V. Rotation in ITB Plasmas

ITBs have been formed with off-axis ICRF heating [41,47-49] and also occur in purely Ohmic plasmas (see Chapter IV). Parameter time histories for a typical ITB discharge are shown in Fig.20. This 4.5 T, 770 kA plasma entered H-mode at 0.671 s after application of 2 MW of 80 MHz ICRF power (the resonance location was near $r/a = 0.5$ on the high magnetic field side), as evidenced by the increases in the plasma stored energy, central electron density, central electron and ion temperatures and core toroidal rotation velocity. Just before 0.9 s, the velocity began

to drop (and eventually reverse direction) and the central electron density began to increase, indicating the ITB formation. One candidate process for the ITB production mechanism is the suppression of turbulence via strong shear in the plasma rotation [51]. Clearly toroidal rotation is involved in the ITB development process in Alcator C-mod plasmas [41,47], as shown in Fig.20, even though the rotation generating mechanism is unknown. The time history of the toroidal rotation velocity profile for the discharge of Fig.20 is shown in Fig.21. Immediately following the H-mode transition, the velocity increased at the edge of the plasma and propagated inward on a time scale similar to the energy confinement time (see Fig.16 top). The evolution of the toroidal velocity profile between 0.67 and 0.80 s is consistent with pure momentum diffusion from an (unknown) edge source, and a momentum confinement time of ~ 70 ms, about a factor of two larger than the energy confinement time. The velocity reached a maximum of ~ 35 km/s (co-current) by 0.8 s, with a relatively flat profile. The ITB began to form around 0.87 s, at which time the velocity profile inside of the ITB foot ($r/a < 0.5$) collapsed (reduced from a substantial co-current speed to near zero) in about 200 ms. Outside of the ITB foot ($r/a = 0.6$), the velocity decreased on a longer time scale, but didn't reduce to zero or reverse direction. The time evolution of the radial electric field profile can be estimated from this crude toroidal rotation velocity profile using the calculated neo-classical [37] impurity rotation. E_r determined in this fashion is demonstrated in Fig.22, along with the corresponding pressure (total ion and electron) profiles. The electric field was positive in the core of the plasma during the normal EDA H-mode phase, then reversed direction in the core as the ITB evolved. During the ITB phase, E_r varied in sign (from negative to positive) moving outward in the vicinity of the ITB foot, suggesting a negative E_r well. A lower limit to the electric field gradient of 250 kV/m² was determined near the maximum of the pressure gradient; this could be a factor of ~ 3 higher. While neither the cause for the co-current toroidal rotation in the initial H-mode phase nor that of the subsequent reversal in the core as the barrier develops is understood, the observed velocity gradient and inferred electric field gradient are consistent with the workings of velocity shear stabilization of ITG

driven turbulence as the ITB evolves.

VI. Comparison with Theory

Several attempts to explain the observed rotation in C-Mod have been made, based on ICRF wave driven fast particle orbit shift mechanisms [52-55], turbulence [56,57] and sub-neo-classical [58] effects. The similarity of the rotation observed in ICRF and purely Ohmic plasmas suggests that it is not due to ICRF wave or fast particle effects. The prediction of reversal of the rotation direction with high magnetic field side (HFS) off-axis ICRF absorption [53,55] has not been observed in the experiments [41]. For the turbulence driven theories [56,57], the sign of the rotation is correct, but the magnitude cannot be tested because the turbulence fluctuation levels are not measured. The predictions of the rotation magnitude and direction from the sub-neo-classical theory, derived for the high collisionality regime, agree with the measurements [58], but the calculated momentum diffusion time scale is two orders of magnitude longer than what is observed. It's possible for the rotation magnitude and direction to be consistent with (sub-)neo-classical predictions while the magnitude of the perpendicular momentum diffusivity is off by orders of magnitude. There are many instances where aspects of parallel transport are in agreement with neo-classical theory, such as the bootstrap current or impurity asymmetries [59], whereas perpendicular transport coefficients are orders of magnitude off, such as heat, momentum or impurity diffusivities.

One approach toward explanation of the co-current rotation in ICRF heated H-mode discharges is through the toroidal torque provided by the radial electric field arising due to orbit shifts of high energy ions generated by ICRF waves [52-55]. A particular prediction of some of these theories [53,55] is that the rotation should switch direction to counter-current with the ICRF resonance located on the high magnetic field side (HFS). The resonance location has been moved by varying the toroidal magnetic field [41,47]. Shown in Fig.23 is a comparison of two H-mode discharges [60] produced by 1.5 MW of ICRF power at 70 MHz. For the

plasma shown by the solid lines, the resonance was on the magnetic axis for 4.5 T and there were the usual characteristics of stored energy increase and co-current rotation. The discharge shown by the dash-dot lines (4.0 T) exhibited very similar co-current rotation even though the resonance location was $(R-R_0)/a \sim -0.4$ on the HFS, in contrast to the predictions. Operation with the ICRF resonance outside of $|r/a| = 0.5$ led to the discovery of ITB plasmas in C-Mod [41,47], however. The similarities in the rotation observations (magnitude and scalings) in Ohmic and ICRF heated H-mode plasmas suggest that it is not an ICRF wave or fast particle effect.

An alternative approach to explain the spontaneous generation of rotation is based on turbulence. Fluctuation induced toroidal stress [56] can give rise to toroidal rotation and the direction of the rotation depends upon the mode frequency spectrum, which may explain the reversal of the observed rotation in going from L- to H-mode. If the Doppler shifted mode frequency is of order of the ion diamagnetic drift frequency, ω^*_i , the calculated velocity profile is predicted to have a shape proportional to the temperature profile, raised to the 5/2 power (Eq.15 of [56]). This is not what is observed in the profiles for EDA H-mode discharges, as can be seen in the top frame of Fig.24 [60]. The observed flat rotation profile is compared to the measured electron temperature shape raised to the 5/2 power, and the agreement is not good. For the ELM-free H-mode rotation profile in the bottom frame of Fig.24, the agreement is reasonable however. The points (\times s) at $r/a \sim 0.2$ are from sawtooth pre- and post-cursors and are in excellent agreement with the x-ray data.

VII. Discussion and Conclusions

Core rotation velocities have been determined in Alcator C-Mod plasmas from the Doppler shifts of argon and molybdenum emission lines recorded with an array of von Hamos type x-ray spectrometers. C-Mod discharges have no external momentum input. For L-mode plasmas, the rotation is generally found to be in

the counter-current direction (the rotation direction reverses when the plasma current direction is reversed), with argon and molybdenum ions rotating at the same speed. The magnitude of the core L-mode toroidal rotation depends strongly on the magnetic configuration, which is related to the higher H-mode power threshold observed when the X-point is located away from the ion $\mathbf{B} \times \nabla B$ drift direction. In Ohmic and ICRF heated H-modes, the core toroidal rotation is in the co-current direction, with velocities reaching 140 km/s (Mach number 0.3) in some cases, and the core E_r is in the range of +30 kV/m. Again, argon and molybdenum ions rotate with the same velocity, and the rotation reverses direction when the plasma current direction is reversed, to remain co-current in H-mode. The increase of the central rotation velocity after entering H-mode is proportional to the increase of the plasma stored energy, normalized to the plasma current, for both ICRF and Ohmic H-modes. For EDA H-mode discharges, the rotation is seen to propagate in from the plasma edge and the velocity profiles are flat; the time evolution can be modeled with a momentum diffusivity of order 0.07 m²/s, much larger than the neo-classical value, indicating the anomalous nature of momentum transport. For ELM-free H-modes, the velocity profiles are centrally peaked, suggesting the workings of an inward momentum pinch. In EDA H-mode plasmas which develop ITBs, the core rotation velocity is found to decrease and reverse direction, indicating a negative E_r well in the interior.

The observed spontaneous rotation is not likely due to ICRF wave or energetic ion orbit shift effects. Some features are consistent with neo-classical theory, as well as some predictions of turbulence-induced rotation.

VIII. Acknowledgements

The authors thank J. Terry for D_α measurements, C. Fiore for ion temperature measurements, S. Scott for useful discussions and the Alcator C-Mod operations and ICRF groups for expert running of the tokamak. Work supported at MIT by DoE Contract No. DE-FC02-99ER54512.

References

- [1] K.C.Shaing and E.C.Crume, Phys. Rev. Lett. **63** (1989) 2369.
- [2] H.Biglari et al., Phys. Fluids **B2** (1990) 1.
- [3] R.J.Groebner et al., Phys. Rev. Lett. **64** (1990) 3015.
- [4] K.Ida et al., Phys. Rev. Lett. **65** (1990) 1364.
- [5] P.W.Terry, Rev. Mod. Phys. **72** (2000) 109.
- [6] K.Burrell, Phys. Plasmas **4** (1997) 1499.
- [7] E.J.Strait et al., Phys. Rev. Lett. **74** (1994) 2483.
- [8] S.Suckewer et al., Nucl. Fusion **21** (1981) 1301.
- [9] K.H.Burrell et al., Nucl. Fusion **28** (1988) 3.
- [10] S.D.Scott et al., Phys. Rev. Lett **64** (1990) 531.
- [11] A.Kallenbach et al., Plasma Phys. Contr. Fusion **33** (1991) 595.
- [12] N.Asakura et al., Nucl. Fusion **33** (1993) 1165.
- [13] K.Nagashima et al., Nucl. Fusion **34** (1994) 449
- [14] K.-D.Zastrow et al., Nucl. Fusion **38** (1998) 257.
- [15] J.S.deGrassie et al., Nucl. Fusion **43** (2003) 142.
- [16] W.D.Lee et al., Phys. Rev. Lett. **91** (2003) 205003.
- [17] J.E.Rice et al., Nucl. Fusion **38** (1998) 75.
- [18] J.E.Rice et al., Nucl. Fusion **39** (1999) 1175.
- [19] I.H.Hutchinson et al., Phys. Rev. Lett. **84** (2000) 3330.
- [20] J.E.Rice et al., Phys. Plasmas **7** (2000) 1825.
- [21] L.-G.Eriksson et al., Plasma Phys. Contr. Fusion **39** (1997) 27.
- [22] J.-M.Noterdaeme et al., Nucl. Fusion **43** (2003) 274.
- [23] I.H. Coffey, R. Barnsley, F.P. Keenan *et al.*, in Proceedings of the 11th Colloquium on UV and X-ray Spectroscopy of Astrophysical and Laboratory Plasmas, Nagoya, Japan, 1995, p.431, Frontiers Science Series No.15 (Editors: K. Yamashita and T. Watanabe), Universal Academy Press, Tokyo, Japan, 1996
- [24] G.T.Hoang et al., Nucl. Fusion **40** (1999) 913.
- [25] L.-G.Eriksson et al., Nucl. Fusion **41** (2001) 91.

- [26] S.Assas et al., 'Toroidal plasma rotation in ICRF heated Tore Supra discharges', 30th European Physical Society Conference on Plasma Physics and Controlled Fusion, St. Petersburg, Russia, 7-11 July 2003, ECA Vol. **27A** P-1.138
- [27] J.E.Rice et al., Nucl. Fusion **37** (1997) 421.
- [28] J.E.Rice et al., Nucl. Fusion **44** (2004) 379.
- [29] B.LaBombard et al., Nucl. Fusion **44** (2004) 1047.
- [30] I.H.Hutchinson et al., Phys. Plasmas **1** (1994) 1511.
- [31] J.E.Rice et al., Rev. Sci. Instrum. **61** (1990) 2753.
- [32] E.S.Marmor et al., Rev. Sci. Instrum. **72** (2000) 940.
- [33] L.L.Lao et al., Nucl. Fusion **25** (1985) 1611.
- [34] E.S.Marmor et al., Phys. Rev. A **33** (1986) 774.
- [35] J.E.Rice et al., Phys. Rev. A **51** (1995) 3551.
- [36] J.E.Rice et al., J. Phys. B **29**(1996) 2191.
- [37] Y.B.Kim et al., Phys. Fluids **B3** (1991) 2050.
- [38] S.P.Hirshman and D.J.Sigmar, Nucl. Fusion **21** (1981) 1079.
- [39] J.A.Snipes et al., Nucl. Fusion **28** (1988) 1085.
- [40] R.J.Buttery et al., Nucl. Fusion **39** (1999) 1827.
- [41] J.E.Rice et al., Nucl. Fusion **41** (2001) 277.
- [42] M.Greenwald et al., Nucl. Fusion **37** (1997) 793.
- [43] J. E. Rice et al., Fusion Eng. Des. **34** and **35** (1997) 159.
- [44] J. Kim et al., Phys. Rev. Lett. **72** (1994) 2199.
- [45] F.L.Hinton and S.K.Wong, Phys. Fluids **28** (1985) 3082.
- [46] F.H.Seguin et al., Phys. Rev. Lett. **51** (1983) 455.
- [47] J.E.Rice et al., Nucl. Fusion **42** (2002) 510.
- [48] S.J.Wukitch et al., Phys. Plasmas **9** (2002) 2149.
- [49] J.E.Rice et al., Nucl. Fusion **43** (2003) 781.
- [50] A.Hubbard et al., Plasma Phys. Contr. Fusion **40** (1998) 689.
- [51] R. E. Waltz et al., Phys. Plasmas **2** (1995) 2408.
- [52] C.S.Chang et al., Phys. Plasmas **6** (1999) 1969.
- [53] F.W.Perkins et al., Phys. Plasmas **8** (2001) 2181.

- [54] V.S.Chan et al., Phys. Plasmas **9** (2002) 501.
- [55] L.-G.Eriksson and F.Porcelli, Nucl. Fusion **42** (2002) 959.
- [56] K.C.Shaing, Phys. Rev. Lett. **86** (2001) 640.
- [57] B.Coppi, Nucl. Fusion **42** (2002) 1.
- [58] A.L.Rogister et al., Nucl. Fusion **42** (2002) 1144.
- [59] J.E.Rice et al., Nucl. Fusion **37** (1997) 241.
- [60] J.E.Rice et al., Phys. Plasmas **11** (2004) 2427.

Figure Captions

Fig. 1 Top view of Alcator C-Mod with tangentially viewing x-ray spectrometers at C, F and K ports, and nearly perpendicular views at B port.

Fig. 2 X-ray spectra of the Ar^{17+} Ly_α doublet and the $2p^6 - (2p^5)_{\frac{3}{2}}4d_{\frac{5}{2}}$ transition in Mo^{32+} for CCW I_P (dash-dot) and CW I_P (solid) L-mode discharges. The $\text{Ly}_{\alpha 1}$ rest wavelength of $3731.1 \text{ m}\text{\AA}$ is shown by the thin vertical line.

Fig. 3 The rotation velocity time histories for molybdenum (solid) and argon (dash-dot) ions.

Fig. 4 The calculated rotation velocity (dash-dot curves) time histories (from Eq.1) compared to the measured (dots with lines) values, for normal (bottom) and reversed (top) plasma current discharges.

Fig. 5 The plasma stored energy (top frame), electron temperature (middle frame) at the center (above) and $r/a \sim 0.3$ (below) and the toroidal rotation velocity (bottom frame) at $r/a=0.0$ and $r/a=0.3$ for a discharge which developed a locked mode.

Fig. 6 The ambient core toroidal rotation velocity as a function of average electron density for 5.4 T, 0.8 MA plasmas with the ion $\mathbf{B} \times \nabla B$ drift downward. Dots are for lower single null and asterisks are for upper single null. The \times s are for limited discharges.

Fig. 7 A comparison of the central rotation velocity (top) and the distance between the primary and secondary separatrices (bottom) for two discharges with LSN to USN switches.

Fig. 8 The central rotation velocity as a function of SSEP for near double null, 5.4 T, 0.8 MA discharges with an average electron density of $1.4 \times 10^{20} / \text{m}^3$.

Fig. 9 The time histories of several parameters for a 5.7 T, 1.0 MA deuterium H-mode discharge. In the top frame is the plasma stored energy. In the second frame are the central electron density (solid) and the central argon density (dash-dot, $\times 10^4$). In the third frame are the central electron temperature (with sawteeth) and the central ion temperature (smooth). In the fourth frame is the ICRF power and in the fifth frame is the D_α emission. In the bottom frame is the central toroidal rotation velocity of argon ions.

Fig. 10 The dots show the measured argon toroidal (top) and poloidal (bottom) rotation velocities, with error bars. Calculated neo-classical toroidal and poloidal argon rotation velocity profiles, with $E_r=0$, are shown by the lines.

Fig. 11 The time histories of the argon (solid) and molybdenum (dash-dot) toroidal rotation velocities for a 0.85 MA, 5.7 T hydrogen minority discharge. Also shown is the 2.7 MW ICRF pulse.

Fig. 12 A comparison of rotation during ICRF heated plasmas with forward (dashed lines) and reversed (solid lines) plasma current.

Fig. 13 The time histories of the plasma current and ICRF pulse (top frame), plasma stored energy (middle frame) and argon toroidal rotation velocity (bottom frame) for a 0.6 MA discharge (solid lines) and a 1.0 MA discharge (dash-dot lines).

Fig. 14 Trajectories in the W_P - V_{Tor} plane during ICRF heated discharges at 0.6 MA (solid) and 1.0 MA (dash-dot) plasma current (top), and the same trajectories with W_P normalized by I_P (bottom).

Fig. 15 The change in the toroidal rotation velocity (the difference between the H-mode and pre-H-mode values) as a function of the change in the plasma stored energy normalized to the plasma current, for Ohmic and ICRF (with on axis heating) H-modes. The Ohmic values are all shown as dots, regardless of plasma current,

while the ICRF points have different symbols for the various plasma currents: \times s for 1.2 MA, diamonds for 1.0 MA, asterisks for 0.8 MA and triangles for 0.6 MA.

Fig. 16 Comparison of model calculations (solid lines) with observed rotation time histories for an EDA H-mode plasma (top frame) and an ELM-free H-mode plasma (bottom frame). Observations from the plasma center are shown as dots, from $r/a = 0.3$ as asterisks and from $r/a = 0.6$ as diamonds.

Fig. 17 Parameter time histories for a 1.1 MA, Ohmic H-mode discharge. In the top frame is the plasma stored energy, in the second frame is the central electron density, in the third frame is the toroidal magnetic field, in the fourth frame is the plasma current and in the fifth frame is the D_α emission. In the bottom frame is the central toroidal rotation velocity of argon ions.

Fig. 18 Time histories of (from top to bottom) the electron density, ICRF power, electron temperature at the $\Psi=0.95$ surface, electron temperature gradient at the $\Psi=0.95$ surface and the core toroidal rotation velocity for discharges with LSN (green), DN (purple) and USN (red).

Fig. 19 The core toroidal rotation velocity during the L-mode portion of LSN (dots), DN (diamonds) and USN (asterisks) 0.8 MA, 5.4 T discharges with $n_e = 1.4 \times 10^{20}/\text{m}^3$ as a function of SSEP is shown in the top frame. In the bottom is the minimum ICRF power required to induce the L-H transition as a function of SSEP, for several of these same discharges.

Fig. 20 Time histories of (from top to bottom) the plasma stored energy, electron density at $r/a = 0.0$ (solid) and 0.6 (dashed), central electron and ion temperatures, ICRF heating power and central toroidal rotation velocity, for a 4.5 T, 770 kA plasma. The dotted vertical line indicates the time of the L- to H-mode transition.

Fig. 21 Toroidal rotation velocity time histories for $r/a=0$ (dots), $r/a=0.3$ (as-

terisks) and $r/a=0.6$ (diamonds). The H-mode transition was at 0.671 s and the earliest appearance of the ITB was at 0.87 s.

Fig. 22 Plasma pressure (top) and E_r (bottom) profiles for the discharge of Figs.19 and 20. The asterisks represent the radial electric field during the H-mode phase at 0.82 s, while the dots are from the ITB phase at 1.1 s.

Fig. 23 A comparison of two discharges with 1.5 MW of ICRF power at 70 MHz, with on-axis absorption (4.5 T, solid) and with the resonance on the high field side at $(R-R_0)/a \sim -0.4$ (4.0 T, dash-dot). From top to bottom are the plasma stored energies, ICRF waveforms and central toroidal rotation velocities.

Fig. 24 A comparison of toroidal rotation velocity profiles in an EDA H-mode (top) and an ELM-free H-mode discharge (bottom). The solid curves are proportional to $(T_e)^{5/2}$. The points at $r/a \sim 0.2$, shown by the \times s, are from the magnetics measurements.

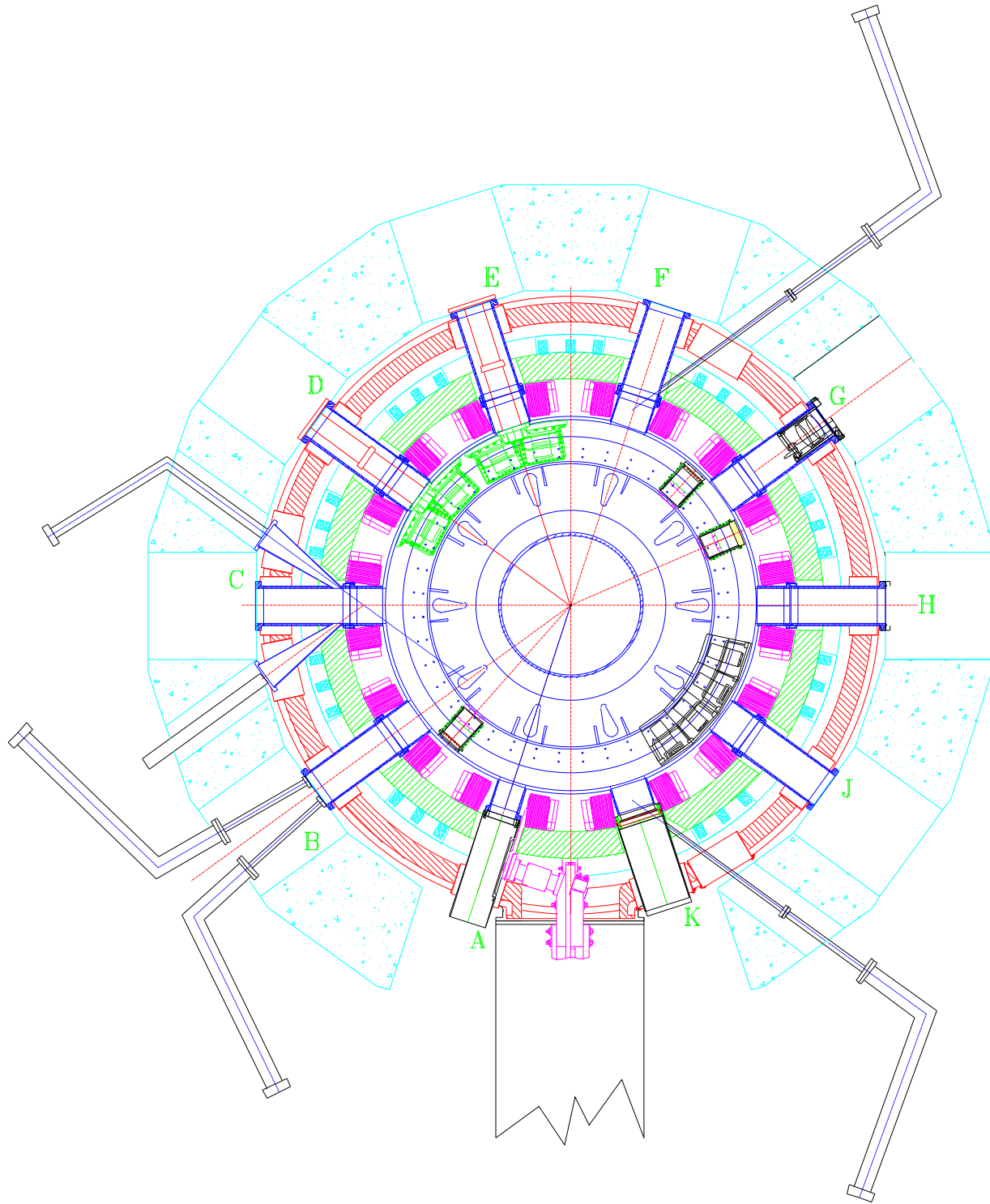


Figure 1

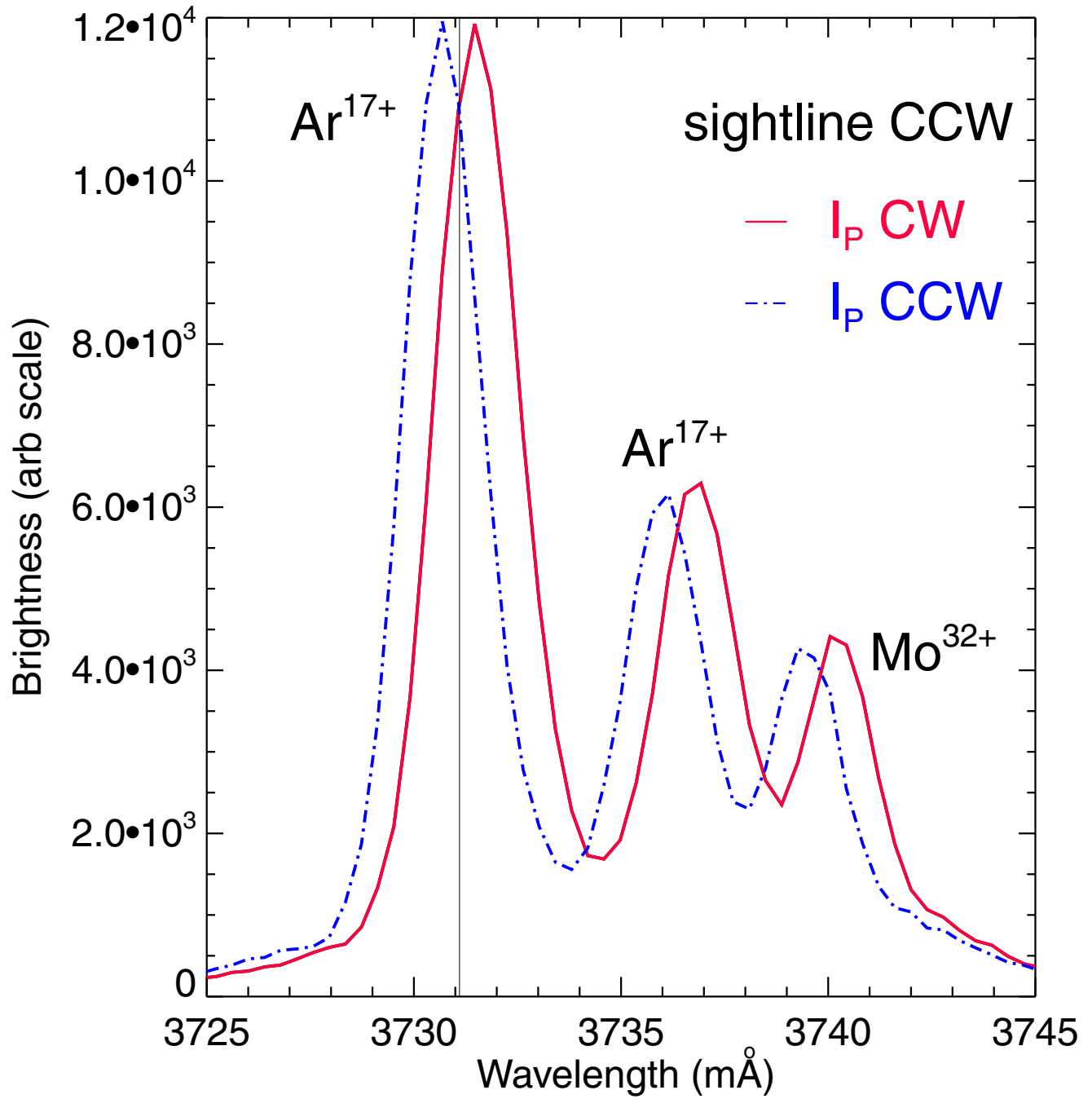


Figure 2

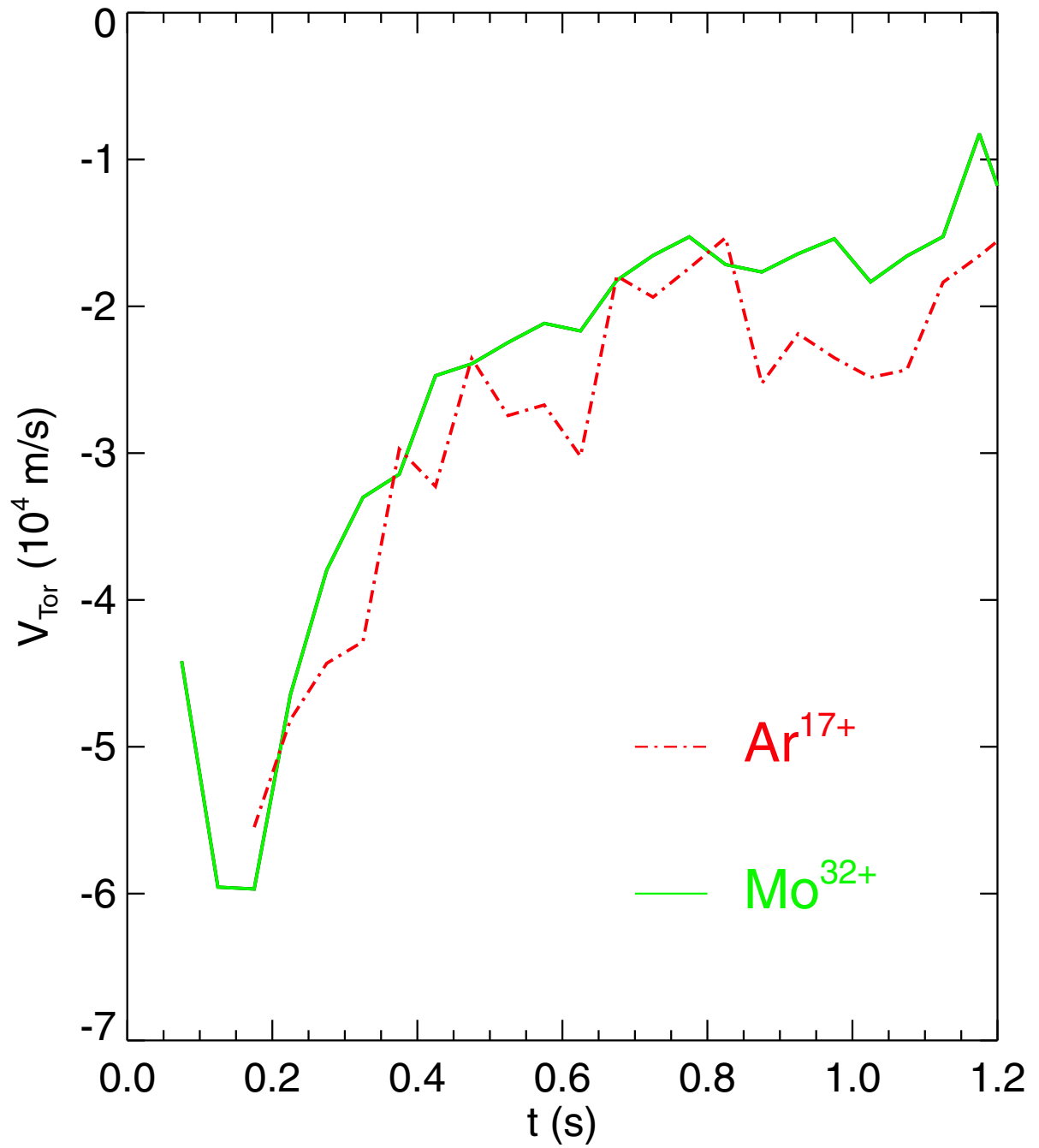


Figure 3

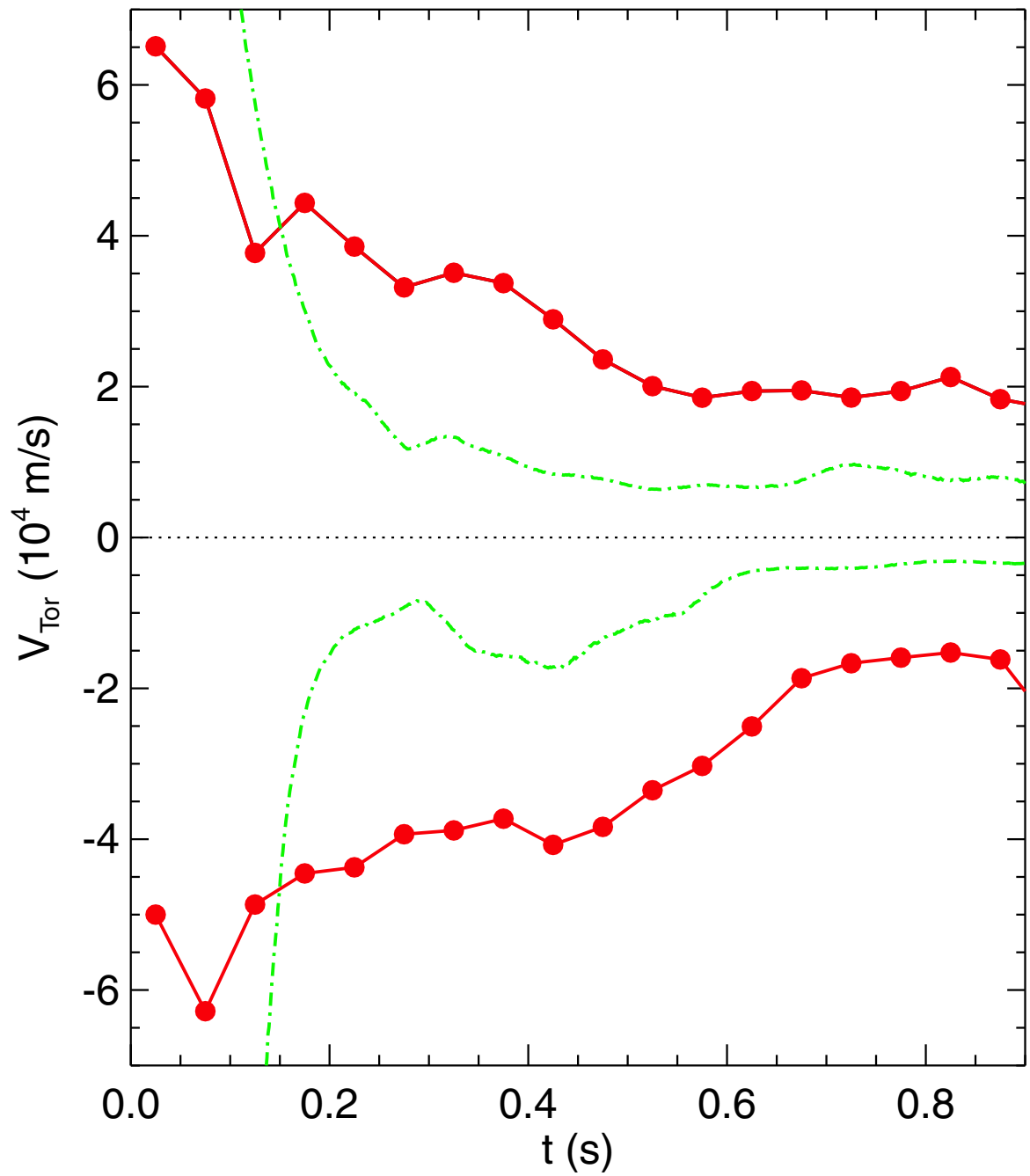


Figure 4

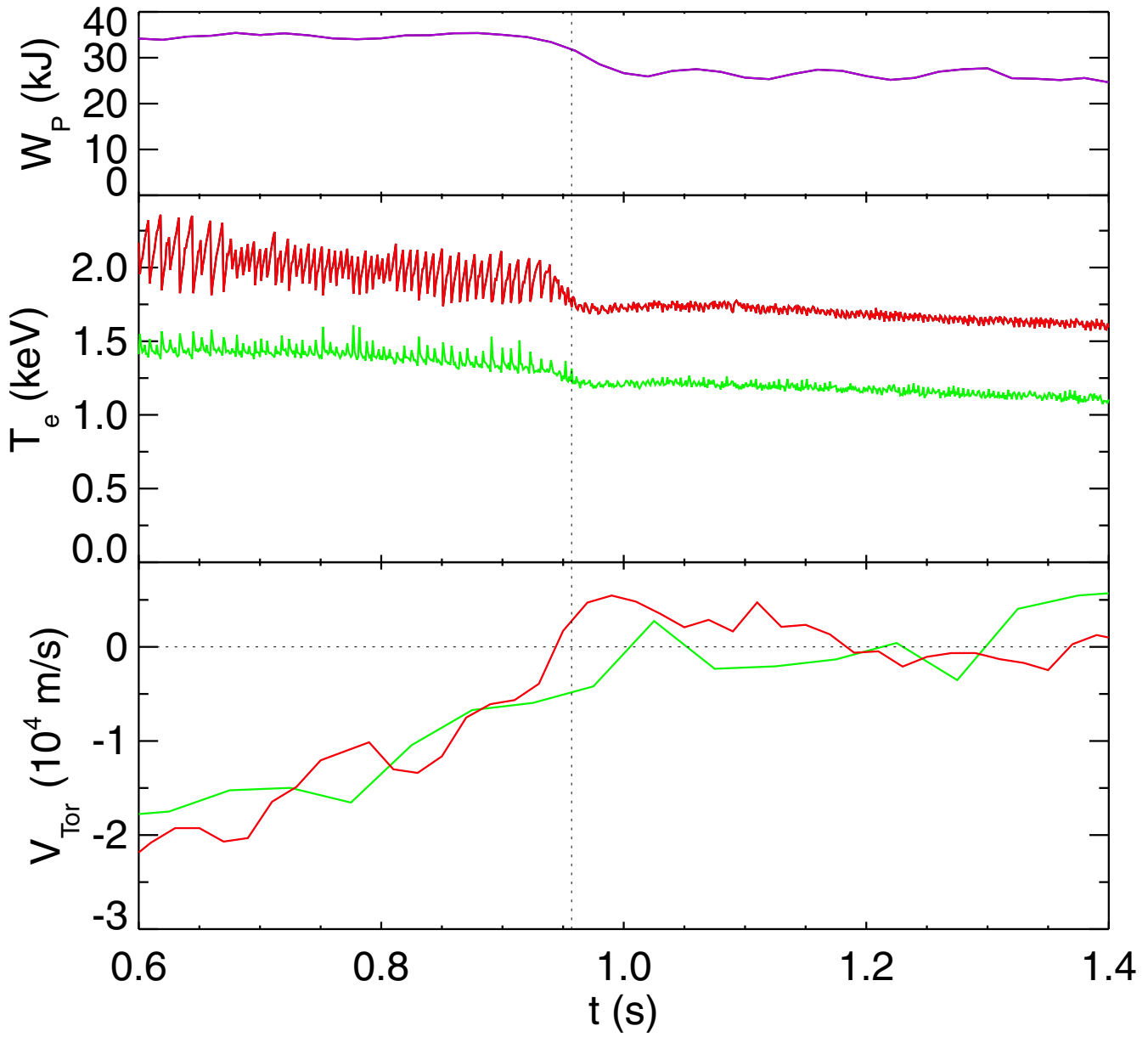


Figure 5

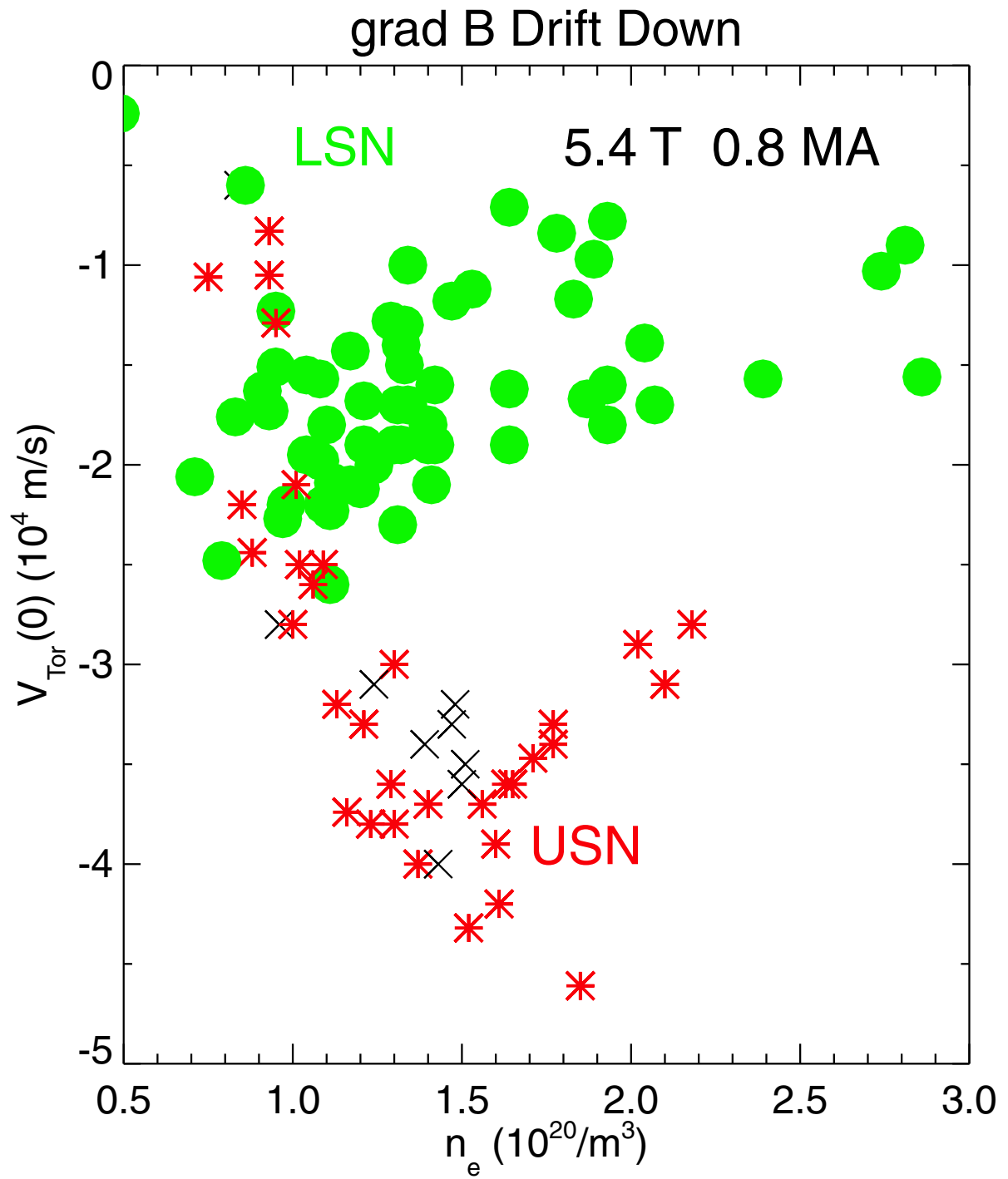


Figure 6

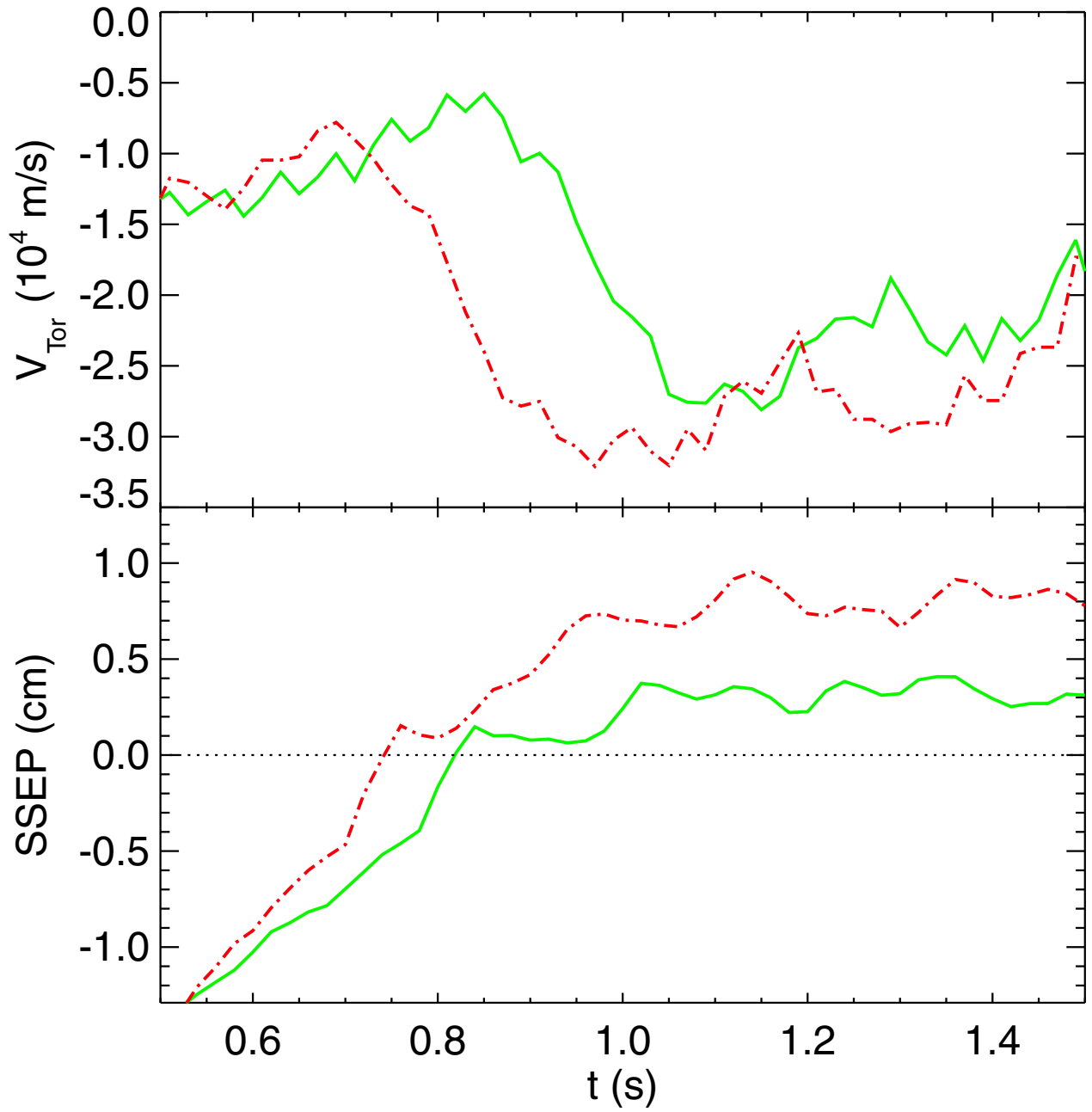


Figure 7

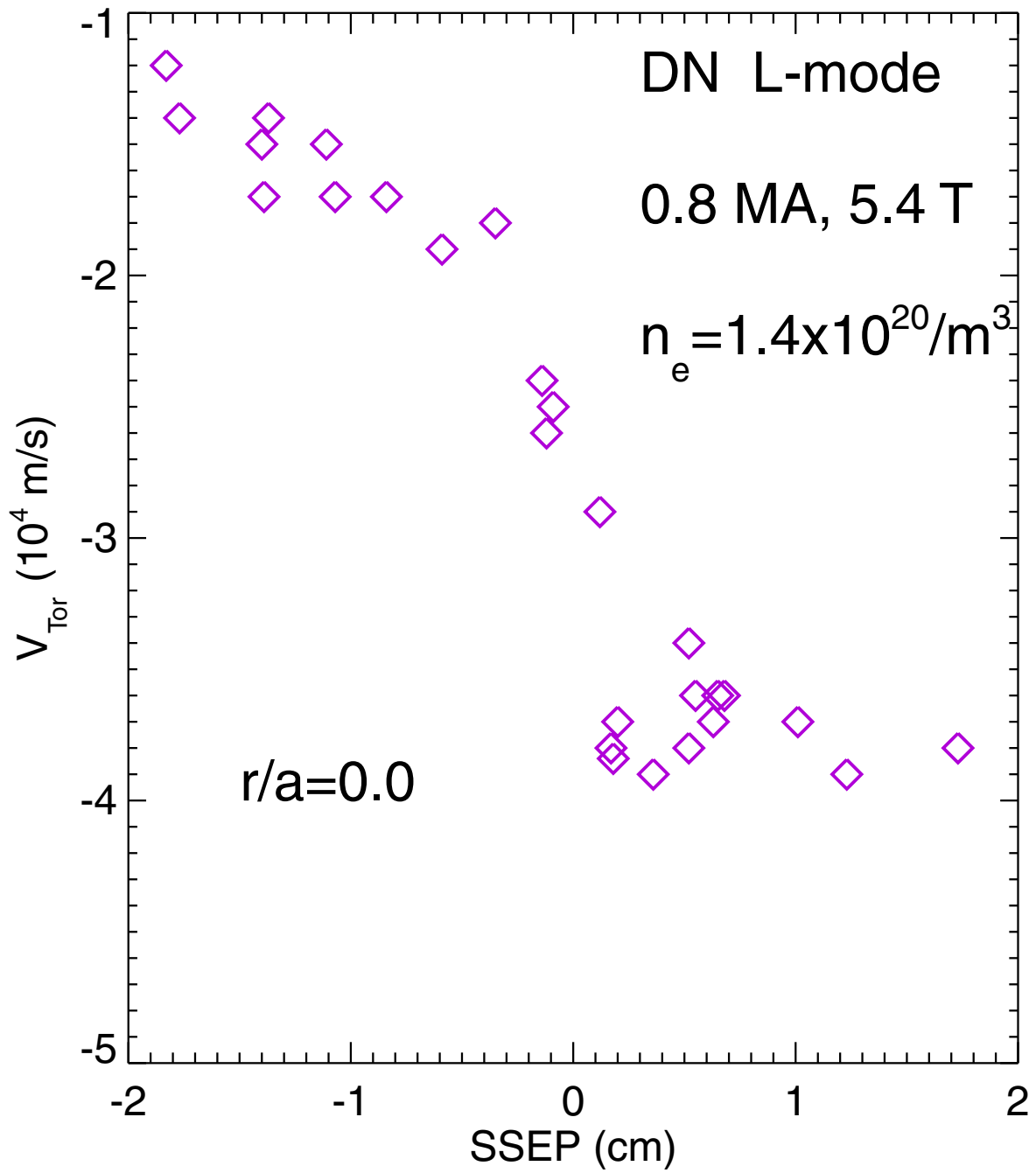


Figure 8

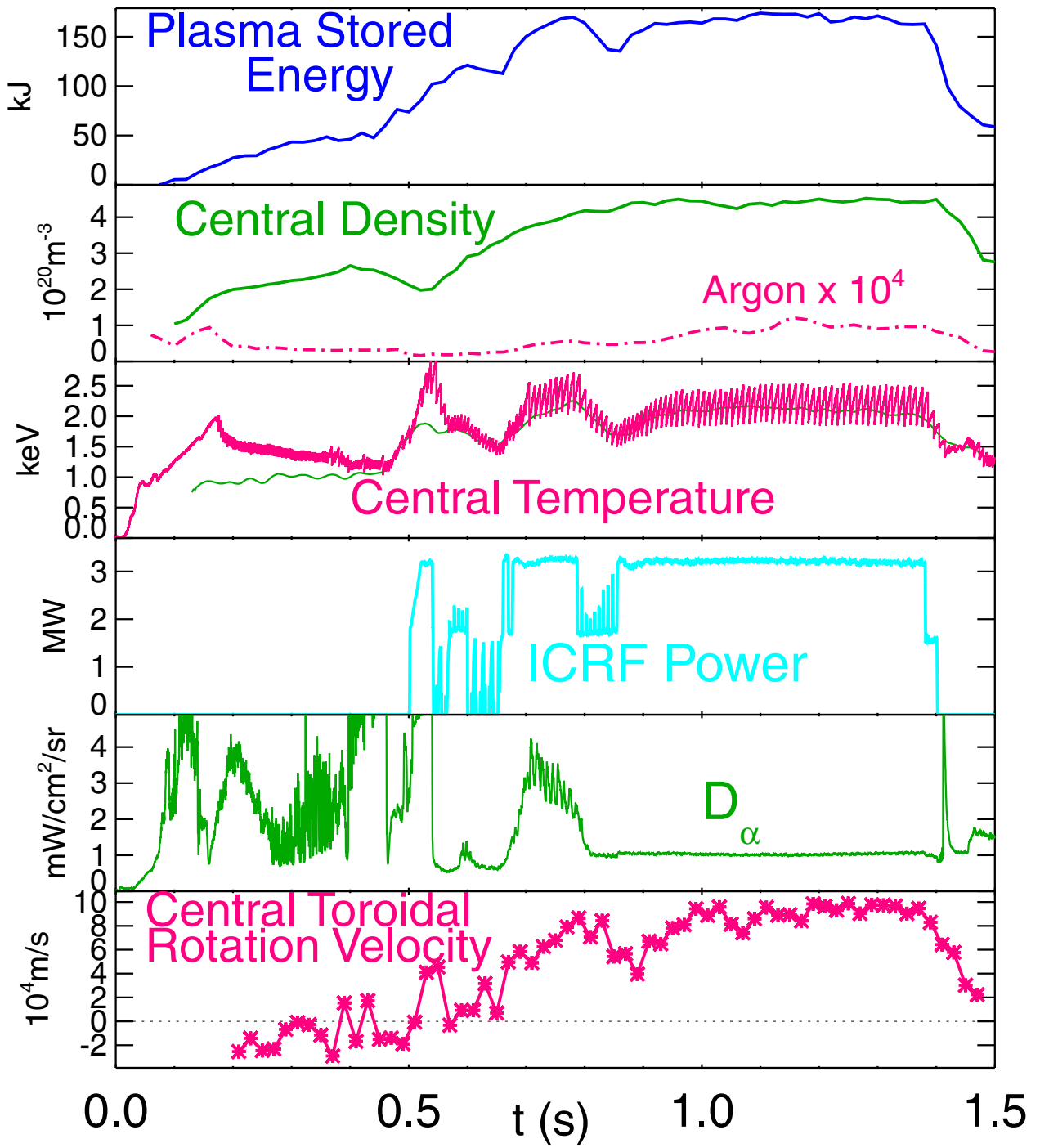


Figure 9

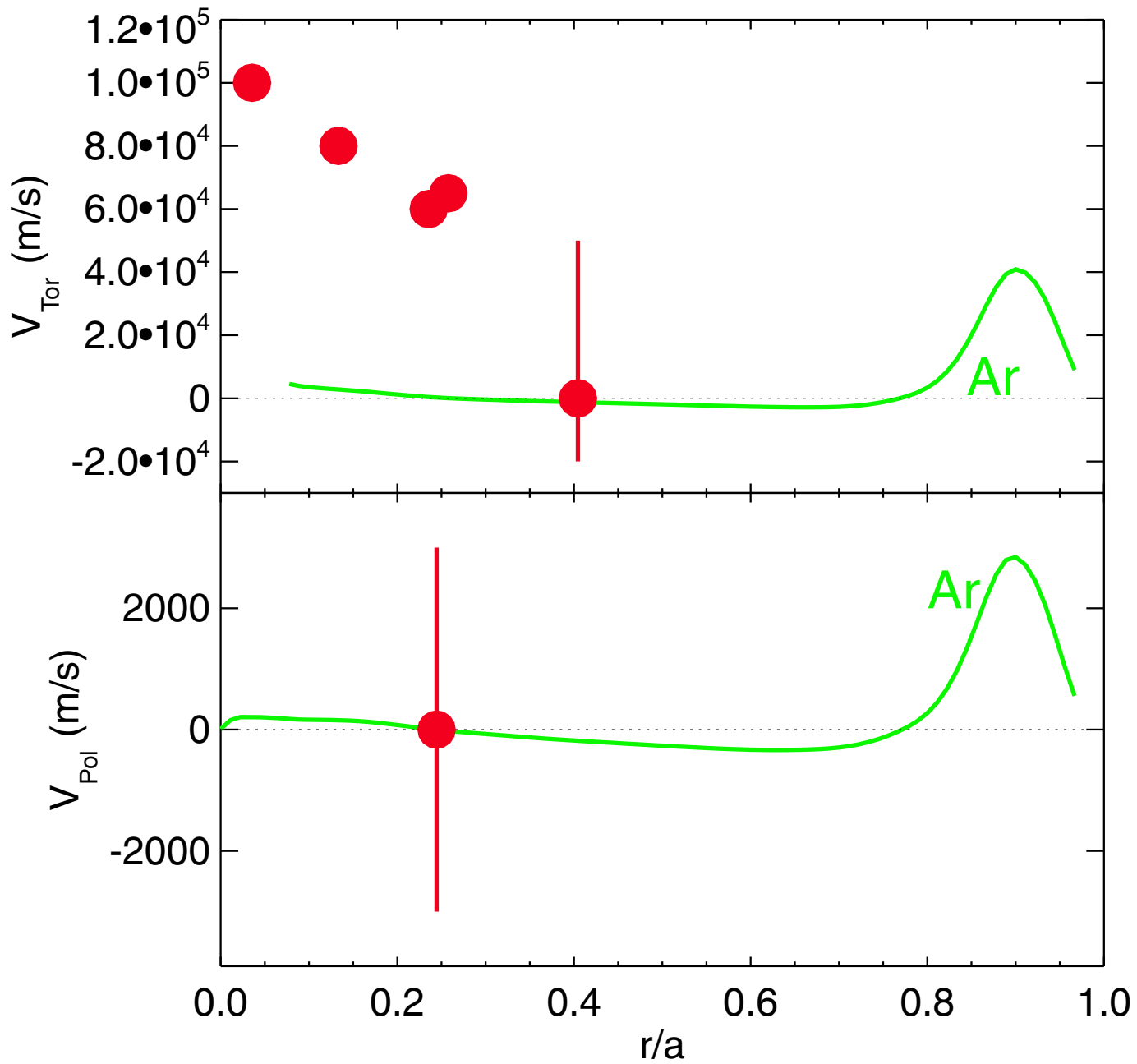


Figure 10

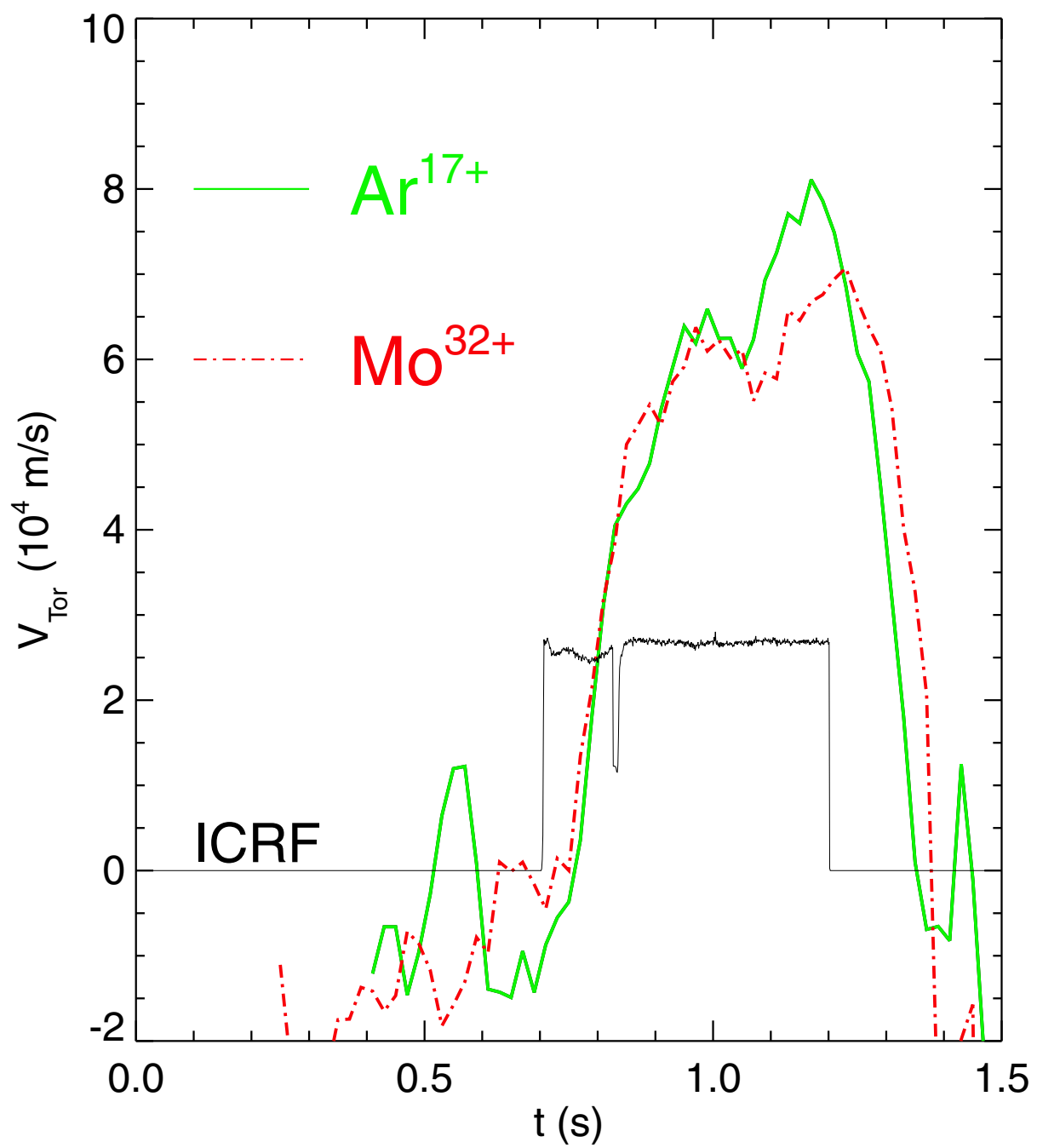


Figure 11

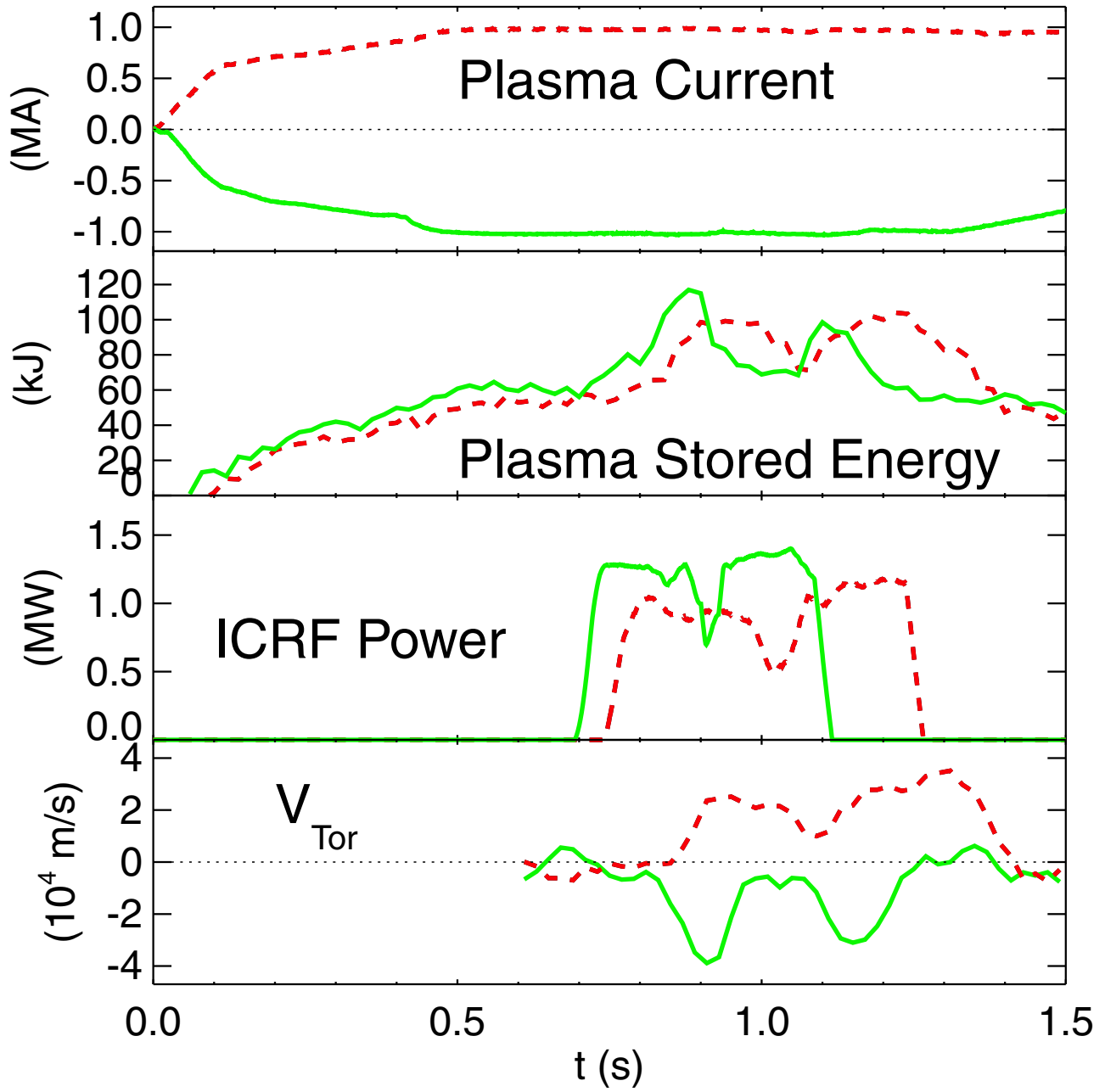


Figure 12

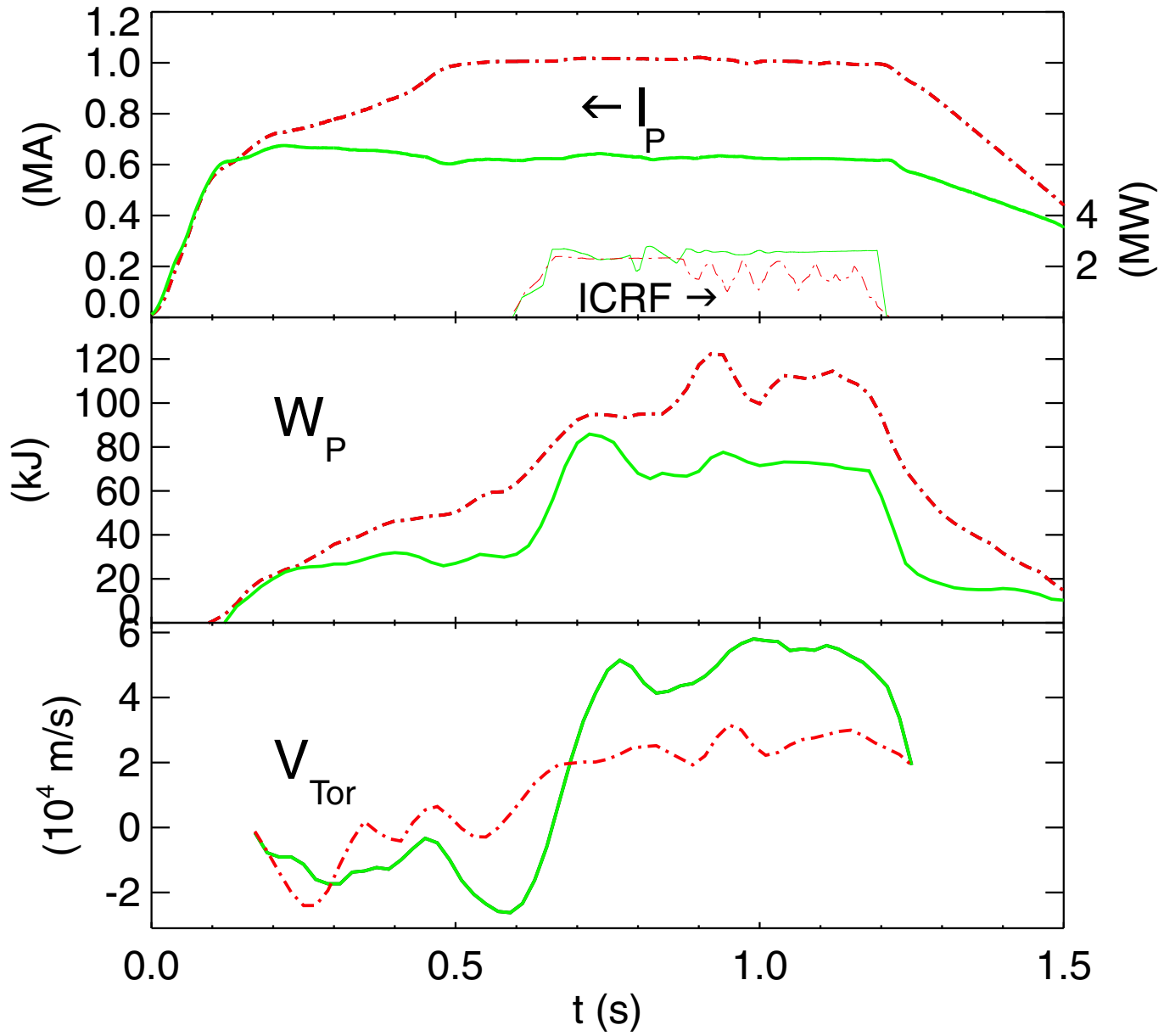


Figure 13

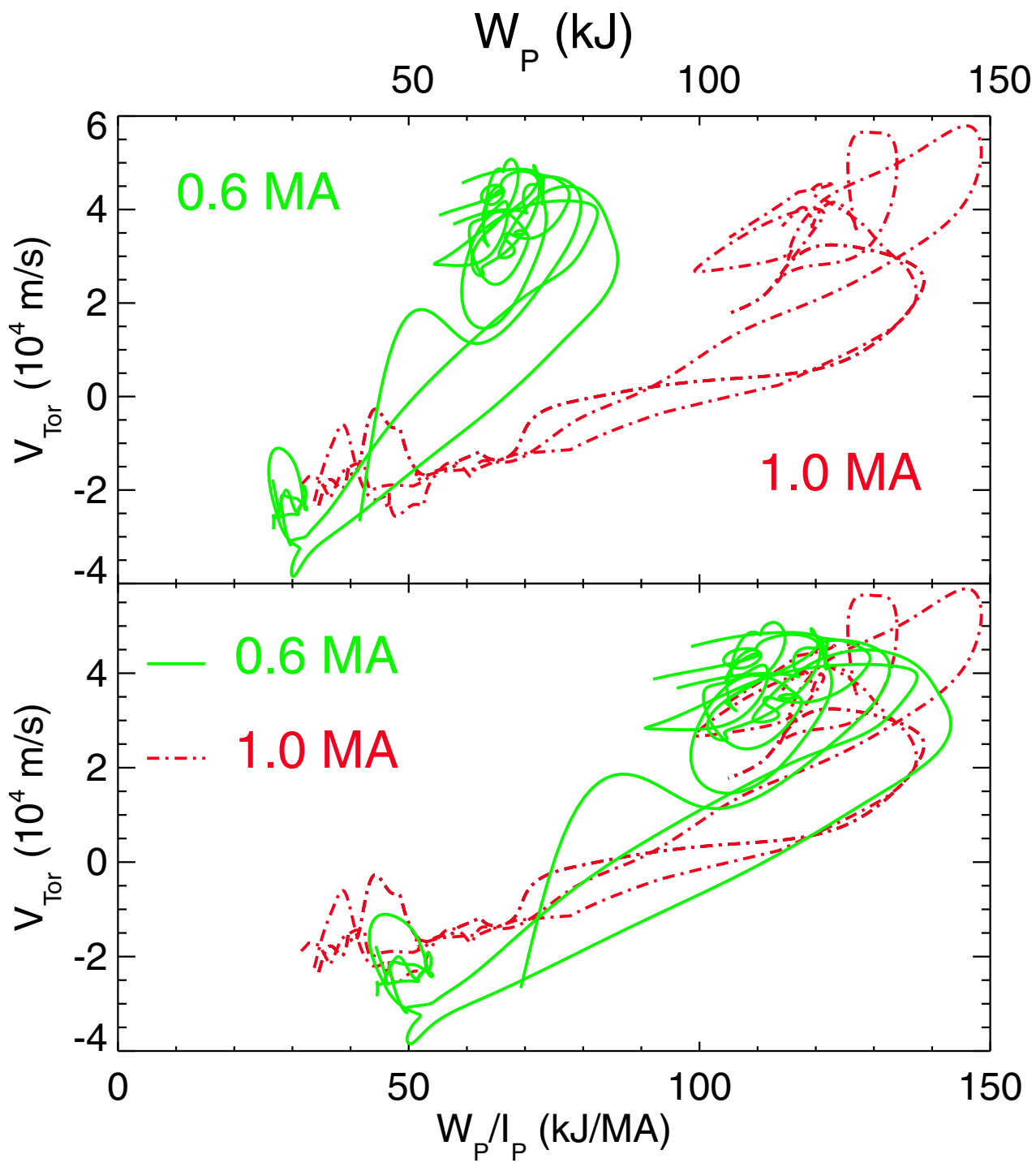


Figure 14

ICRF and Ohmic H-modes

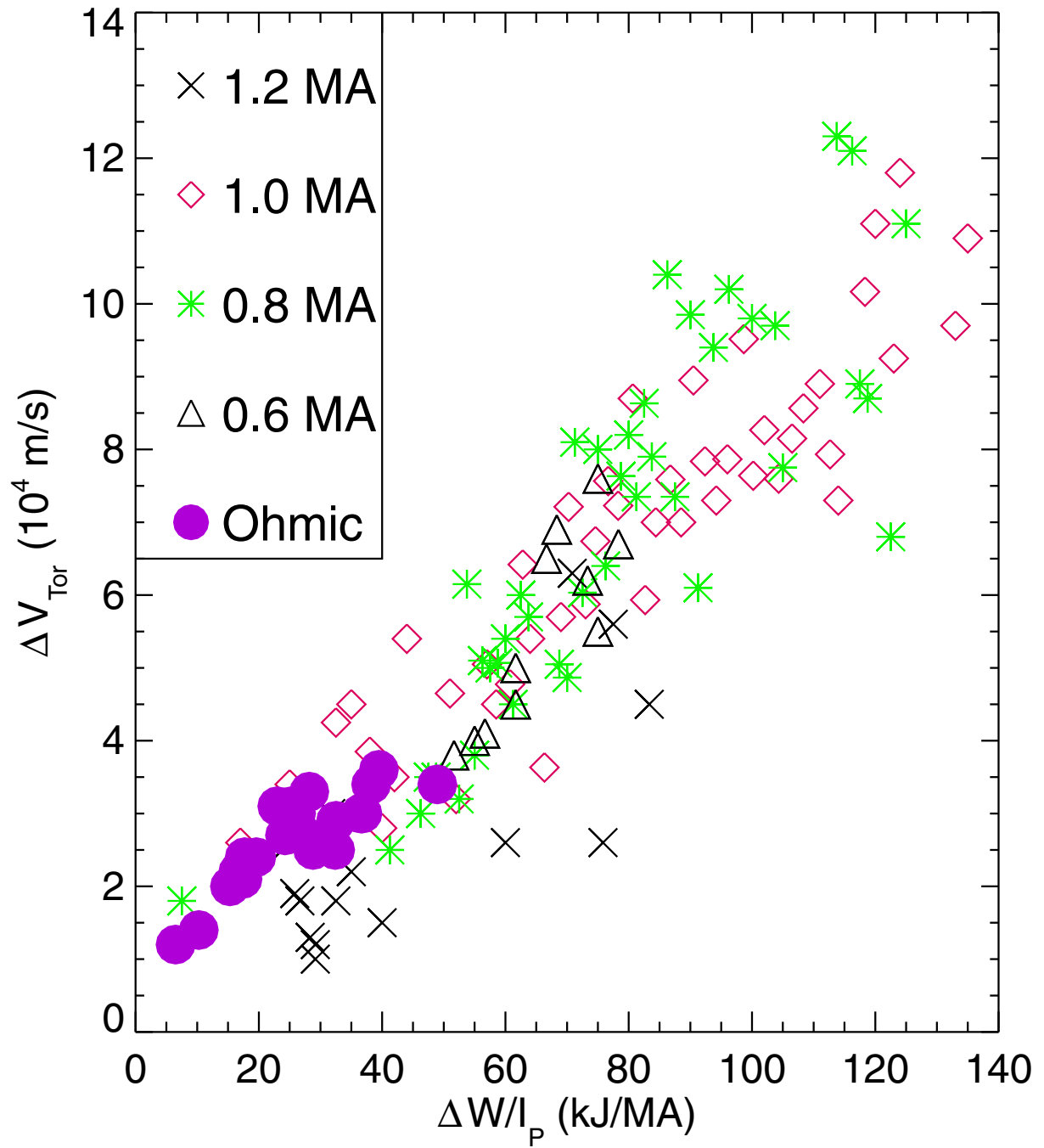


Figure 15

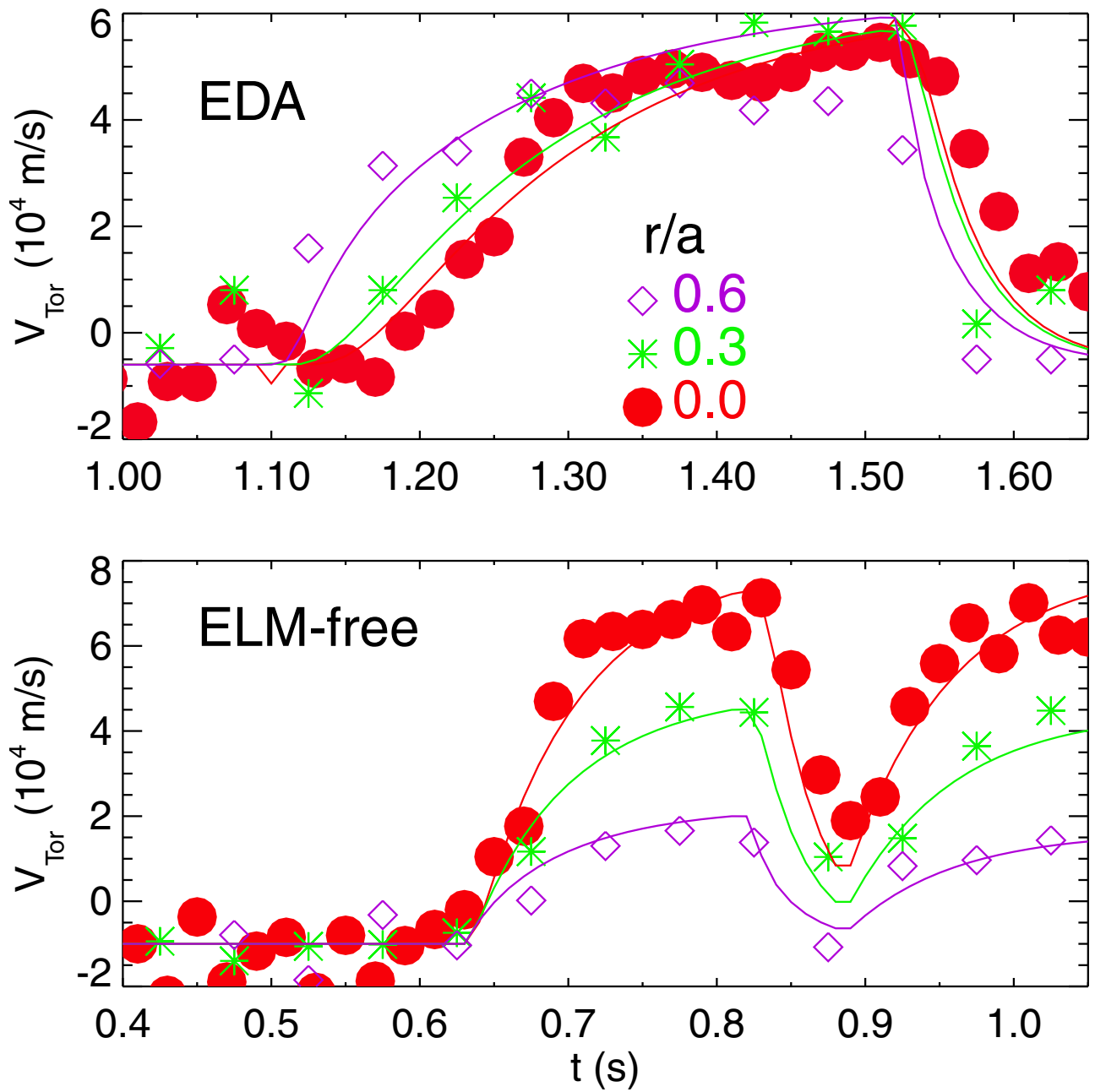


Figure 16

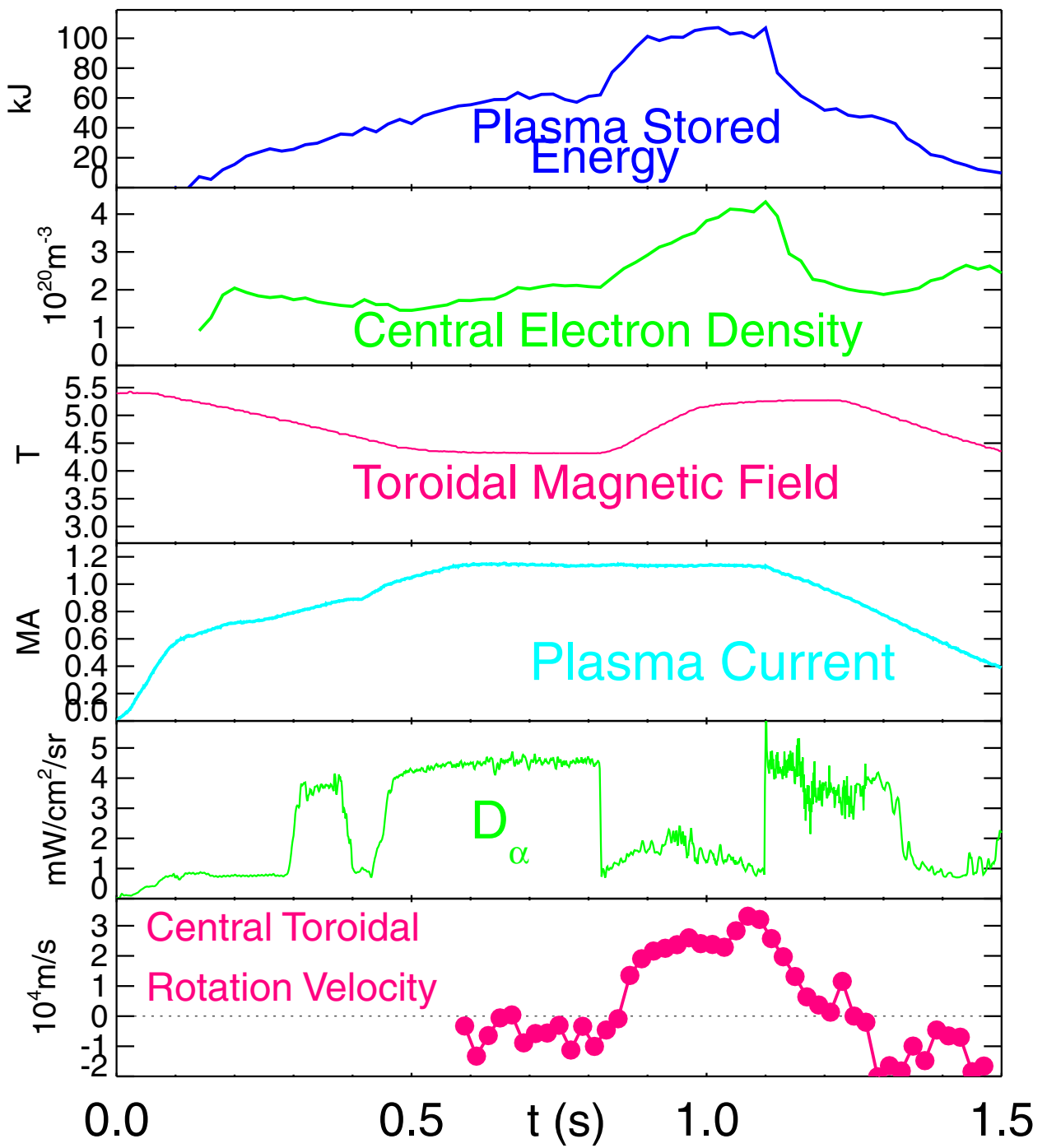


Figure 17

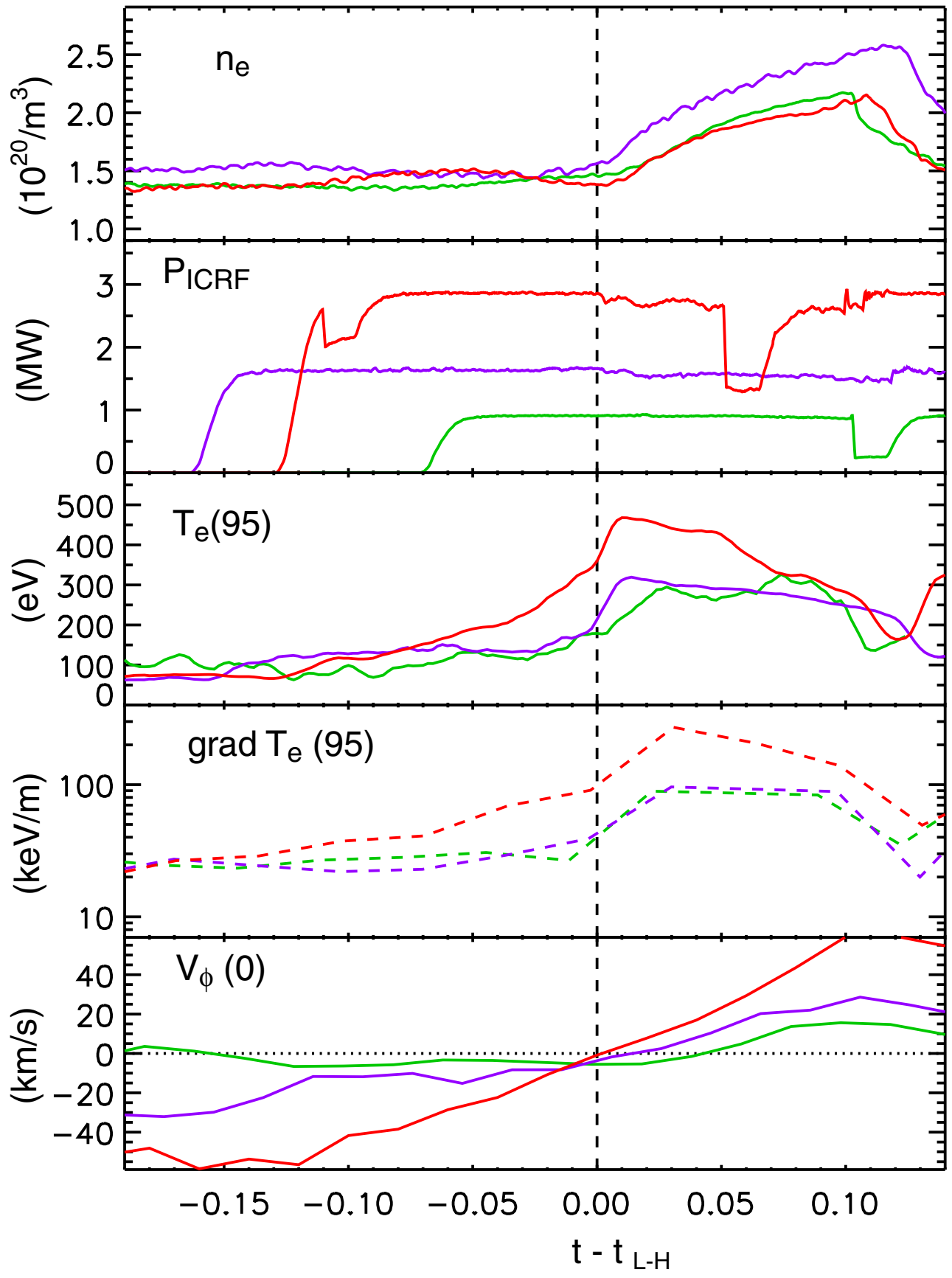


Figure 18

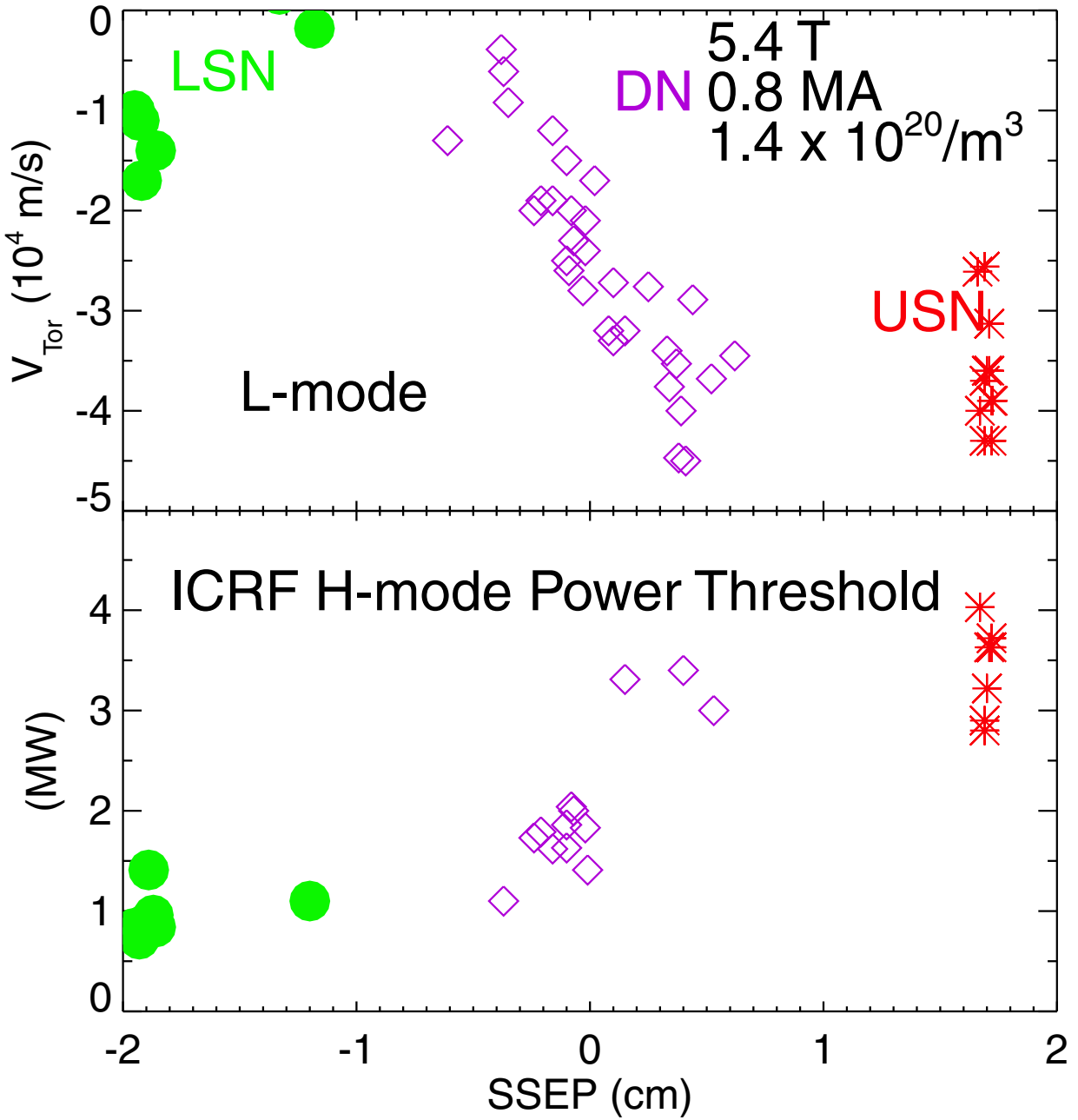


Figure 19

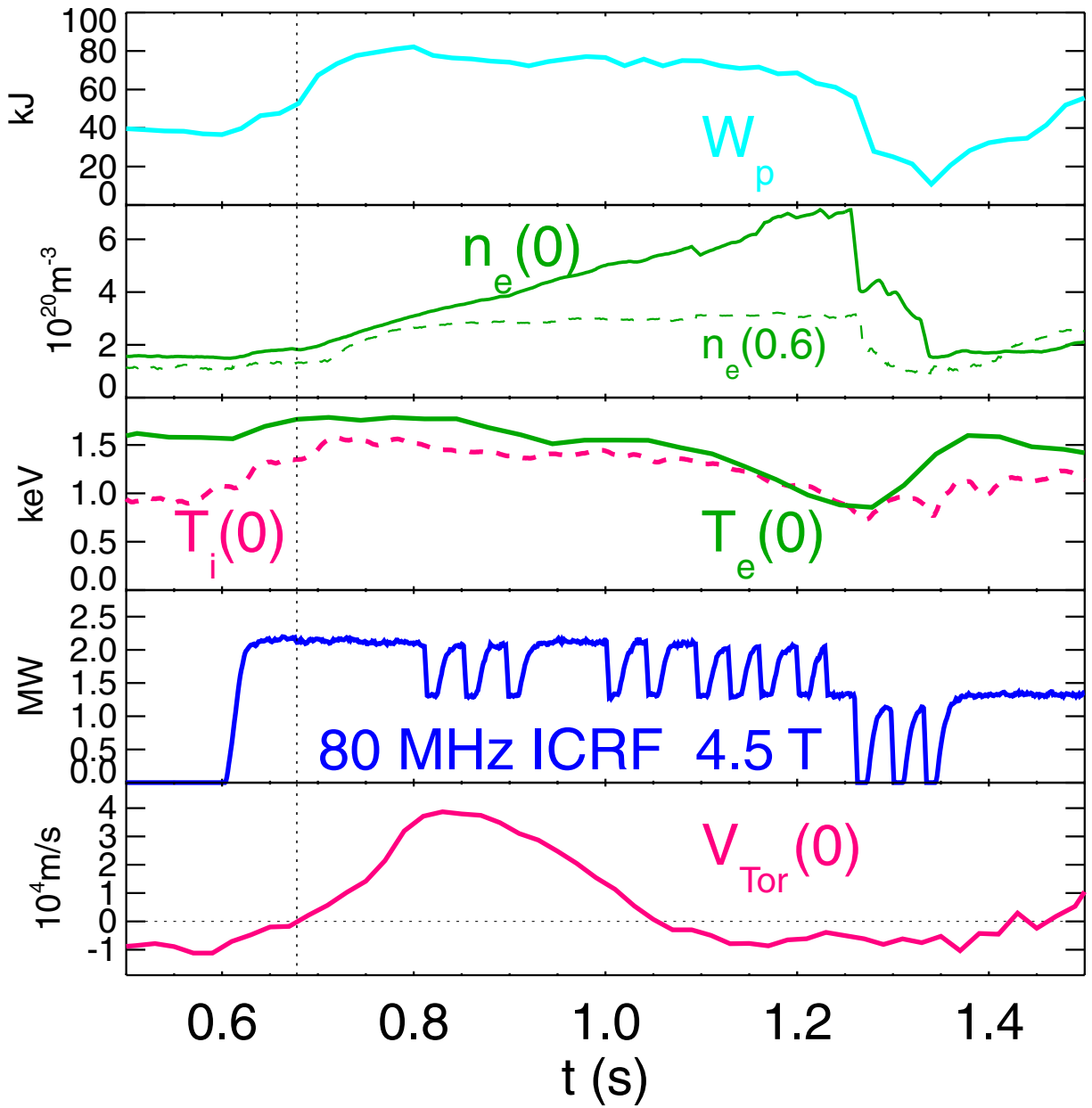


Figure 20

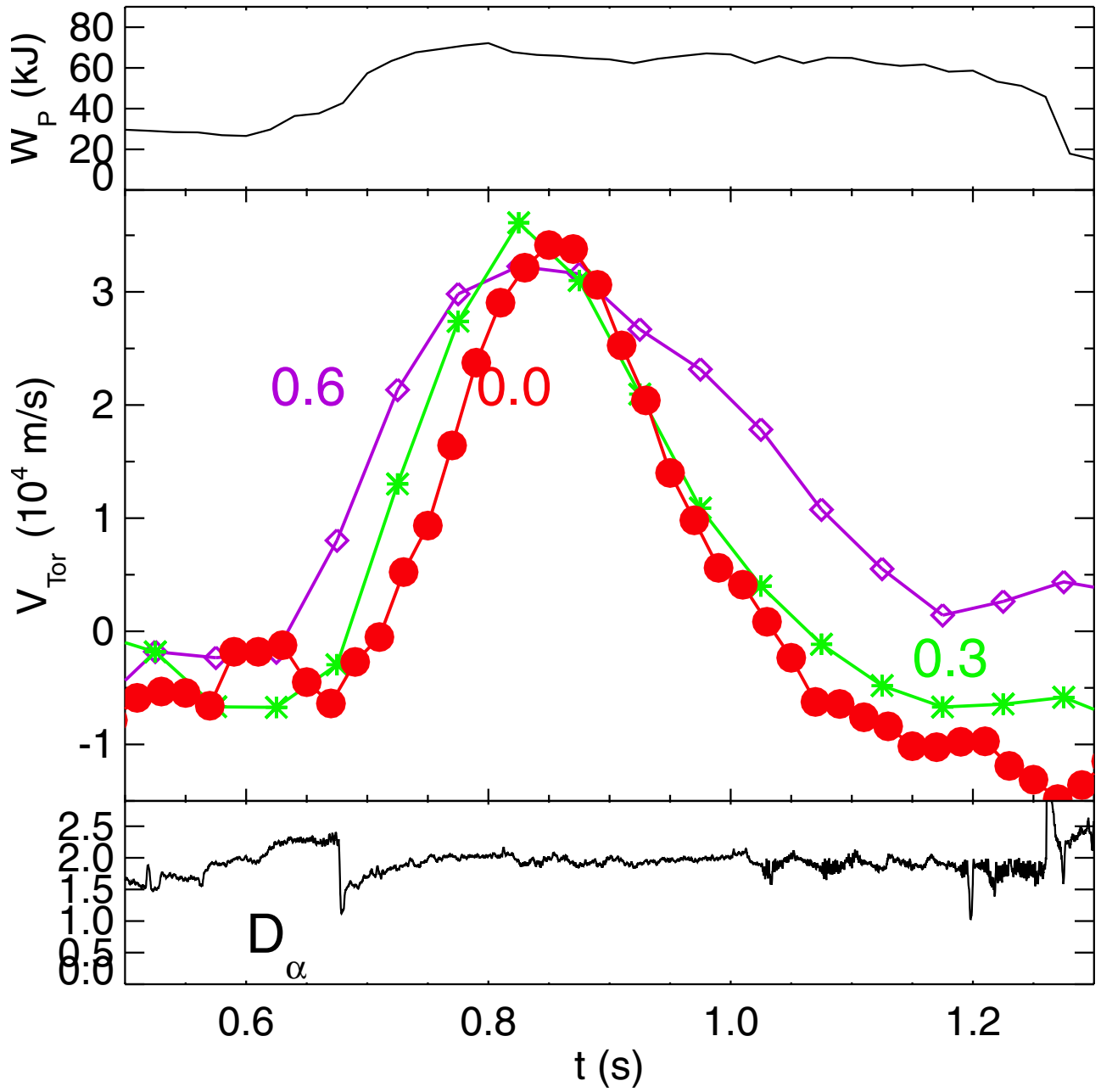


Figure 21

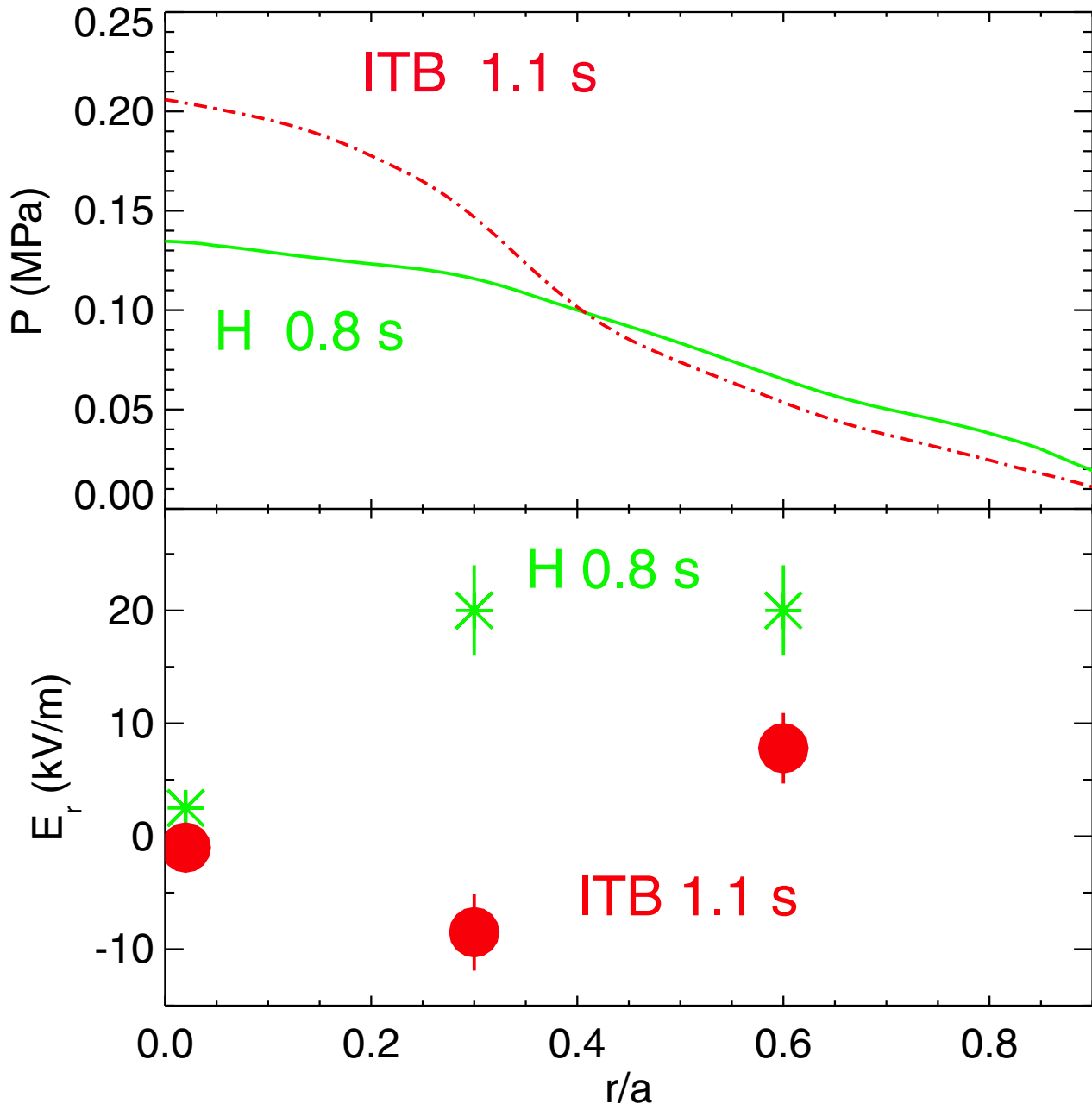


Figure 22

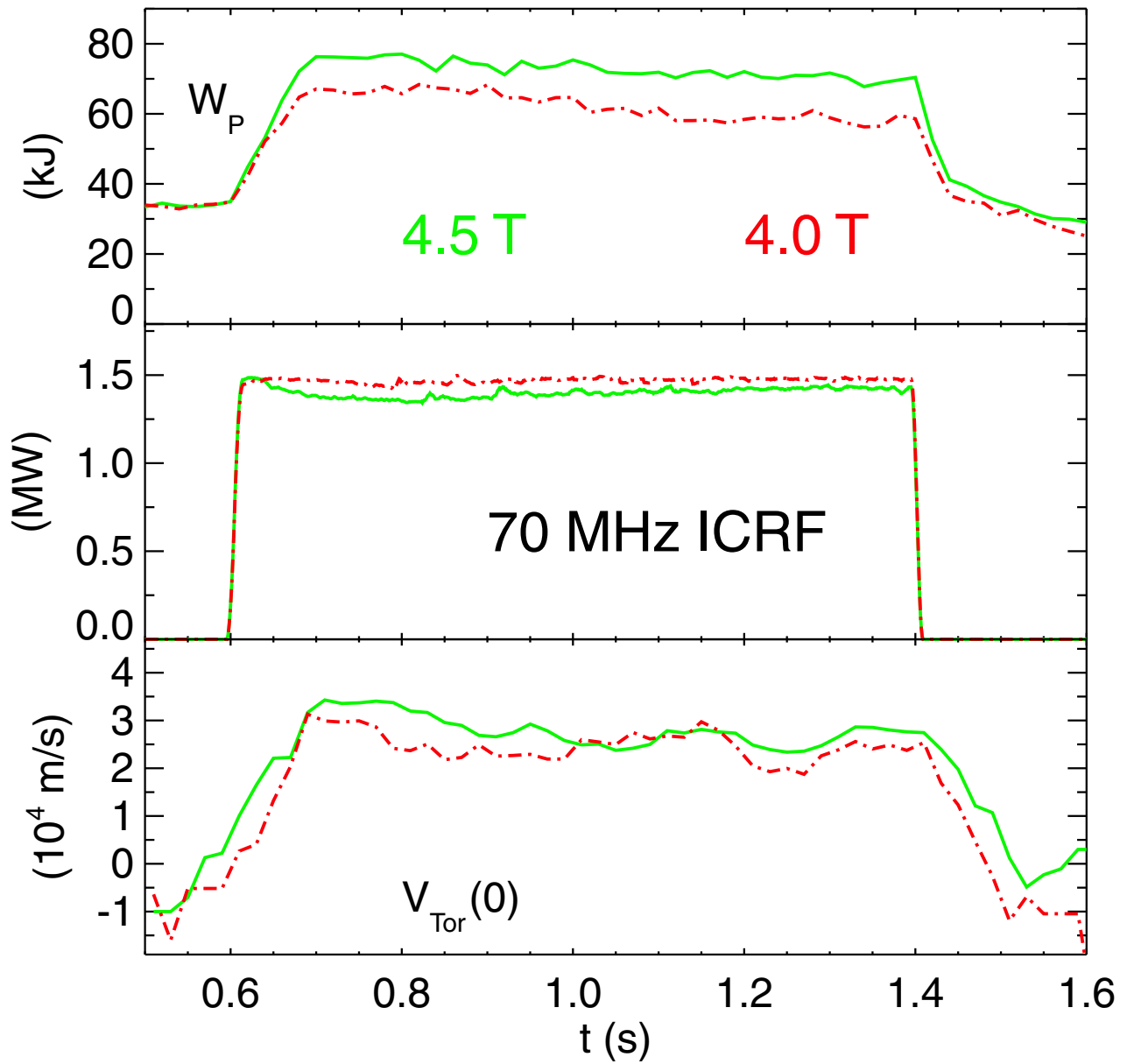


Figure 23

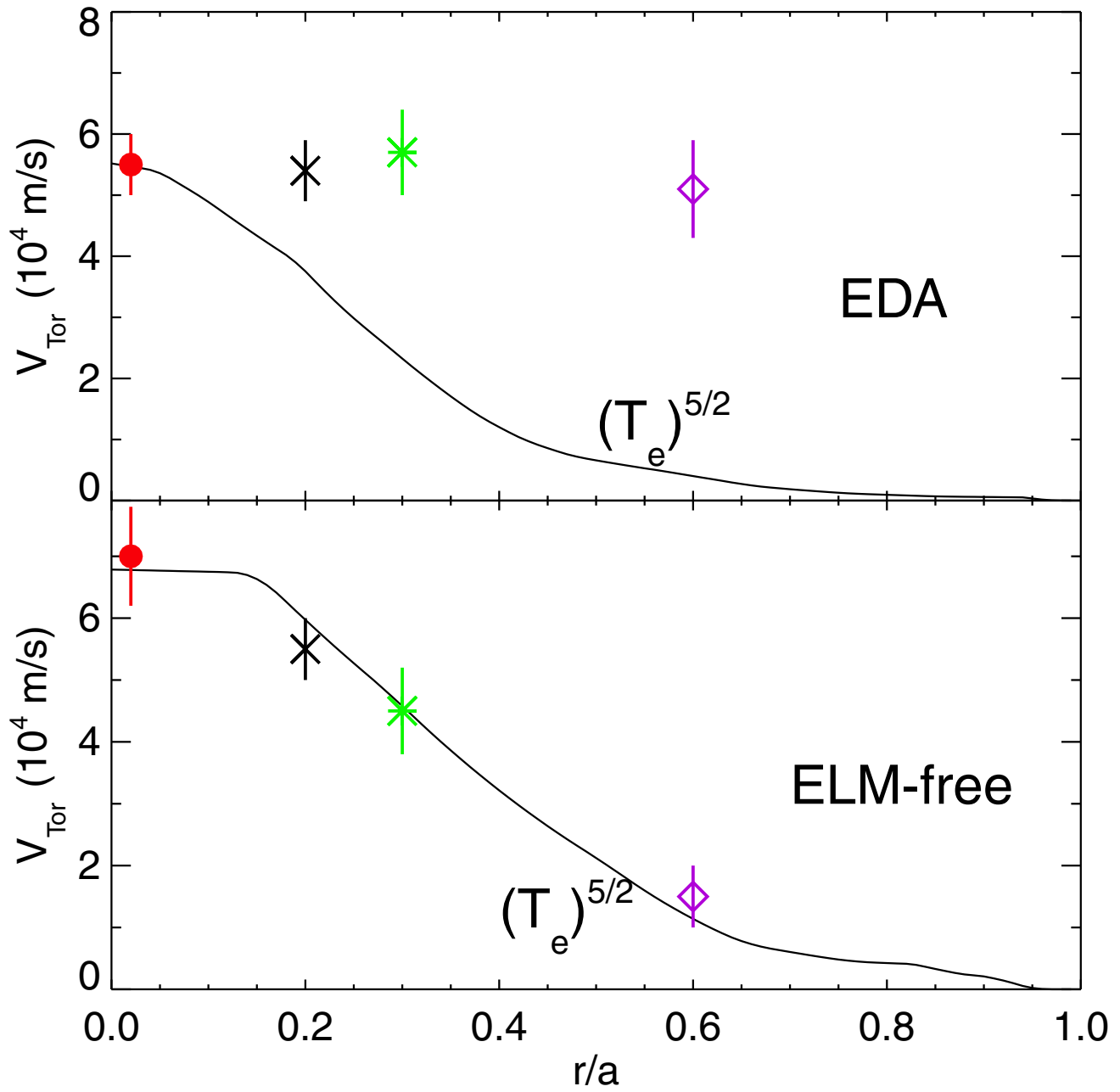


Figure 24